CAMBRIDGE
UNIVERSITY PRESS

Article

Mount Mather Creek, British Columbia – a new sodalite-bearing carbohydrothermal breccia deposit including a new Canadian occurrence for the rare minerals edingtonite and quintinite

Paula C. Piilonen[1]* ⓘ, Glenn Poirier[1], Ralph Rowe[1], Roger Mitchell[2] and Chris Robak[3]

[1]Beatty Centre for Species Discovery, Canadian Museum of Nature, P.O. Box 3443, Station D, Ottawa, Ontario K1P 6P4, Canada; [2]Department of Geology, Lakehead University, Thunder Bay, ON, Canada; and [3]Silver Cove Ltd, Red Deer, Alberta T4L 2R2, Canada

Abstract

The Mount Mather Creek sodalite-bearing carbohydrothermal breccia dyke is located ~35 km northwest of Golden, British Columbia, Canada, within the Foreland Belt on the eastern side of the Mississippian-to-Devonian British Columbia Alkaline Province. The dyke occurs *in situ* on the western side of the Mount Mather Creek gully, cropping out over a distance of ~80 m with a thickness of up to 10 m, intruding a syncline of Middle and Upper Cambrian Chancellor Group carbonate rocks. To date, no parental alkaline complex has been found adjacent or proximal to the dyke. The breccia dyke is flow-banded and matrix-supported and consists of host rock clasts, medium- to coarse-grained, anhedral-to-poikilitic carbonate-rich syenite segregations that occur as veins and pods, and fine-grained banded sodalite plus carbonate fragments in a carbonate-rich matrix. The sodalite-carbonate segregations consist dominantly of sodalite, ferroan dolomite, calcite and microcline, with an extensive suite of trace minerals enriched in rare earth elements (REE), Na, Ba and Sr, including albite, analcime, ancylite-(Ce), chabazite-Na, fluorapatite, baryte, barytocalcite, cancrinite, galena, goethite, gonnardite, harmotome, edingtonite, a potentially new Mg-bearing edingtonite-like mineral, natrolite, nordstrandite, pyrite, quintinite and sphalerite. Alteration of the primary silicate–carbonate assemblage has resulted in a secondary assemblage of hydrothermal or carbohydrothermal REE–Ba–Sr–Na phases including albite, analcime, cancrinite, gonnardite and nordstrandite after sodalite, together with complex intergrowths of ancylite-(Ce), barytocalcite, edingtonite, and a potentially-new Mg-bearing edingtonite-like mineral. Remobilisation of Ba and Sr from barytocalcite resulted in crystallisation of late-stage baryte and Sr-rich calcite. Mount Mather Creek is only the fifth Canadian occurrence of the Ba-zeolite, edingtonite, and the second Canadian occurrence of the rare layered double hydroxide quintinite. The Mount Mather Creek breccia is a carbohydrothermal deposit, the product of a low temperature (<450°C), highly evolved, alkaline, SiO_2-undersaturated, Na–Ba–REE–Cl-rich, residual carbonated silicate melt whose parental origins remain unknown.

Introduction

The British Columbia Alkaline Province is a northwest trending belt 150 km wide located along the boundary between the Omineca and Foreland belts of the Canadian Cordillera (Fig. 1) and includes nepheline and sodalite syenite, ijolite, carbonatite, kimberlite, lamprophyre and associated post-magmatic and hydrothermal rocks (Pell, 1994; Hoshino *et al.*, 2017). Exploration for economic deposits of rare earth elements (REE), Nb, Ta and fluorite has occurred within the British Columbia Alkaline Province since the 1950s. However, exploration has been limited, and very few of these deposits have

been studied enough to estimate potential reserves or to develop resources (Simandl and Clarke, 2016). With >70% of current global production of REE originating from People's Republic of China, and >90% of the worlds Nb coming from Brazil, disruptions in supply have become a concern for both Europe and North America (Natural Resources Canada, 2021). It has become imperative that Canada, which has some of the largest known reserves and resources of REE and Nb+Ta in the world, position itself as a 'global supplier of choice' of the critical elements required for a green, low-carbon, high-tech future (Lasley, 2021). Many of the REE prospects in Canada occur in British Columbia, including the Blue River–Upper Fir carbonatite (Ta and Nb), Aley carbonatite (Nb), Wicheeda carbonatite (REE) and the Rock Canyon Creek deposit (REE, F, Ba, Au and Ag). Mineralisation occurs in both primary and secondary assemblages, dominantly in veins, dykes and sudations, the result of late-stage carbohydrothermal fluids enriched in Na, F,

Fig. 1. Location of the Mount Mather Creek carbohydrothermal breccia deposit (red star) within the British Columbia Alkaline Province (green field). Other carbonatite and alkaline intrusions within the Province are denoted by yellow diamonds. Modified after Simandl *et al.* (2021).

Cl, Nb, light REE (LREE), Ba and Sr derived from the parental carbonatite or syenite bodies.

Located ~35 km northwest of Golden, British Columbia, and 64 km northwest of the Ice River Alkaline Complex, the Mount Mather Creek sodalite claim (BC Minfile No. 082N 090; 51° 32′60.00″N, 116°53′12.00″W) lies high above the chalky white waters of the Blaeberry River in a steep gully cut by Mount Mather Creek. Mount Mather Creek is one of the latest intrusions to be described in detail from the British Columbia Alkaline Province. In August 2021, Canadian Museum of Nature researchers were granted access to the claim to study its mineralogy in detail for the first time, allowing us to shed light on its petrogenesis and relationship to other alkaline complexes in the British Columbia Alkaline Province. It is host to a suite of rare and unique Ba–Sr–REE minerals and is only the fifth Canadian locality for the rare Ba-zeolite, edingtonite, and the second Canadian locality for the rare layered double hydroxide, quintinite. The Mount Mather Creek deposit was described originally as a sodalite syenite (Hora and Hancock, 1996). However, closer examination reveals that it has more in common with late-stage carbonatitic dykes and sudations observed in other complexes of the British Columbia Alkaline Province, including the Rock Canyon Creek deposit breccias (Pell, 1994; Green *et al.*, 2017; Hoshino *et al.*, 2017), and with late-stage Fe-rich carbonatites observed worldwide (Drüppel, 2003; Schultz *et al.*, 2004; Drüppel *et al.*, 2005; Al Ani and Sarapää, 2013; Cooper *et al.*,

2015). This paper will describe the geology and mineralogy of the Mount Mather Creek sodalite claim as well as shed light on its paragenesis and relationship to other alkaline intrusions in the British Columbia Alkaline Province.

History

Known only to a few prospectors and provincial geologists, the Mount Mather Creek claim has been revived and is now producing bulk lapidary material. The claim is accessible *via* the Blaeberry Forest Service Road which stops abruptly at a washed-out bridge at Mount Mather Creek. Access to the claim is possible only during summer and autumn due to high flow in the creek during the spring snow melt season.

The deposit was first worked for sodalite prior to 1957 however details of the original miners are not known. In 1957, the new claim owner discovered an old adit was already in place and discussions with local residents in the area have suggested that the miners were searching for lead and zinc during World War II (R. Barkwill, *pers. comm.*). The presence of accessory sphalerite and galena may have originally been of interest to the prospectors, however it would have been quickly determined that there was not sufficient economic tonnage at the locality.

In 1996, the claims were optioned by Dave Lefurgey, who did extensive prospecting in the gully and surrounding valleys (1996–1998). Lefurgey noted that no sodalite syenite float was observed
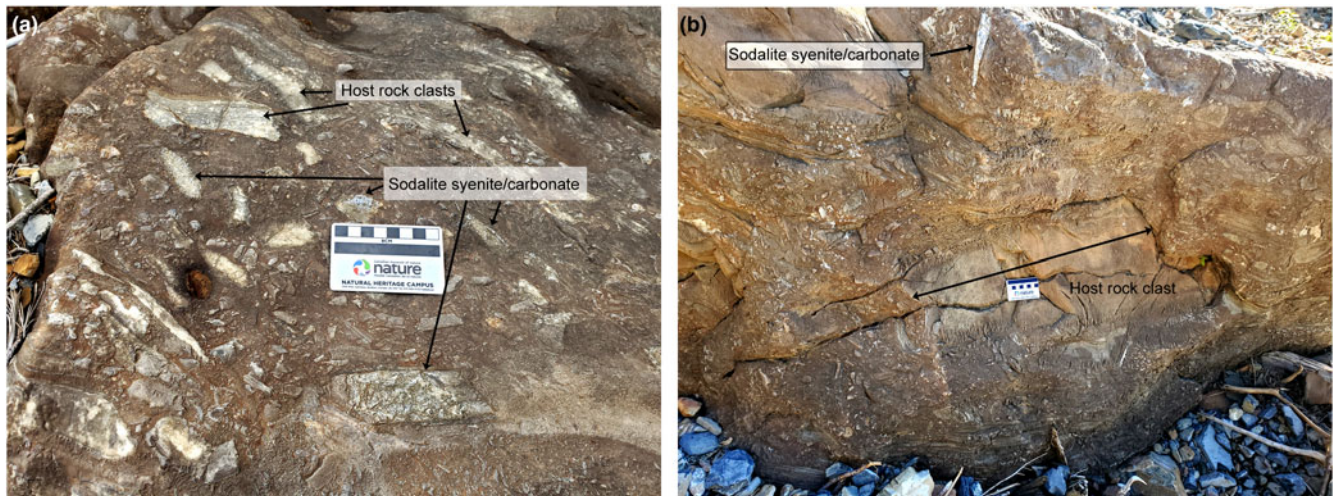
Fig. 2. (a) Mount Mather Creek breccia depicting host-rock clasts and sodalite syenite segregations within a carbonate-dominant matrix. (b) Large host-rock clast and a large sodalite syenite segregation in the Mount Mather Creek breccia.

on the western side of the ridge, in Mount Laussedat Creek (Hora and Hancock, 1996), confirming that the sodalite occurrence is limited to Mount Mather Creek. Currie (1976) had noted occurrences of sodalite veins at Mount Laussedat, though given reports by Lefurgey and our current fieldwork, we agree with Hora and Hancock (1996) that Currie was mistaken and that the true occurrence is at Mount Mather Creek. Lefurgey extracted ∼3 tonnes of rough sodalite for the lapidary market. The claim was later staked by Richard Barkwill in the early 2000s, following years of inactivity. The property was essentially forgotten for 10 years, until claimed by Chris Robak in 2020 who extracted 10 tonnes of sodalite-bearing material from float boulders in the creek bed in spring 2021.

General geology

Mount Mather Creek is located within the Foreland Belt on the eastern side of the British Columbia Alkaline Province (Fig. 1), a series of folded and imbricated miogeoclinal metasedimentary rocks which underwent sub-greenschist to greenschist metamorphism during the Columbian orogeny and currently form the Main and Western Ranges of the Rocky Mountains (Gabrielse and Yorath, 1991; Pell, 1994). Alkaline complexes within this belt are of Mississippian-to-Devonian age and include the Ice River Alkaline Complex, the Bearpaw Ridge sodalite syenite, the Aley, Kechika River and Wicheeda carbonatites, and the Rock Canyon Creek REE–F–Ba deposit (Currie, 1976; Pell, 1994; Peterson and Currie, 1994; Simandl *et al.*, 2012; Dalsin *et al.*, 2015; Hoshino *et al.*, 2017). As a group, the alkaline complexes within this belt are enriched in Nb, F and REE relative to occurrences on the western side of the British Columbia Alkaline Province; of the 44 known strategic element deposits in British Columbia, 43 are from the Foreland Belt (Simandl *et al.*, 2012). A common feature observed around alkaline complexes containing carbonatites in this region, including at Mount Mather Creek, is the presence of a yellow–brown alteration halo, visible from the air (Pell, 1994; Hora and Hancock, 1996). Examination of the material from Mount Mather Creek suggests that this alteration halo is caused by the oxidation of pyrite within the host sediments by hydrothermal fluids, as well as the dominance of Fe-rich carbonates within the actual carbonatite.

The Mount Mather Creek breccia dyke occurs within a syncline of Middle and Upper Cambrian Chancellor Group carbonate rocks (Hora and Hancock, 1996). No parental alkaline complex is associated with the dyke, as is the case for other carbonatitic dykes in the British Columbia Alkaline Province (Pell, 1994). The sedimentary host rock has undergone greenschist metamorphism and consists of very fine-grained calcite (50 vol.%), albite (0–50 vol.%), dolomite (10 vol.%) with minor apatite, pyrite and quartz. Bedding is preserved and thicknesses range from 1 to 10 mm. The country rock has been brecciated by a branching dyke-like body consisting of a carbonate groundmass, veins and sudations of carbonate-rich sodalite syenite and metasomatised host rock clasts up to 1 m in length (average 10–15 cm; Fig. 2). The brecciated dykes occur *in situ* ∼400 metres from the road, cropping out over a distance of ∼80 m with a thickness of up to 10 m in the western wall of the gully (Hora and Hancock, 1996). As noted by Lafurgey (pers. comm.) and Hora and Hancock (1996), two smaller, independent dykes, <2 m in width and dominated by feldspar and calcite with only minor sodalite, occur above and below the main body. However, as it is impossible to access the *in situ* occurrence in the cliff face without technical climbing equipment, all macro- and microscopic observations and analyses have been conducted on samples taken from large boulders of float material found in, and adjacent to, the creek. Their proximity to the outcrop in the wall of the gully indicates that they have not been transported any significant distance. Furthermore, sodalite syenite float was not found further up the creek, indicating the dyke to be localised near the adit without a further northern exposure.

The breccia is flow-banded and matrix-supported and consists of subrounded-to-rounded host-rock xenoliths (1 cm to 1 m in length), medium- to coarse-grained, anhedral-to-poikilitic carbonate-rich syenite segregations that occur as veins (0.5–1 cm in width) and pods (up to 10 × 5 cm), and fine-grained banded sodalite plus carbonate fragments in a carbonate-rich matrix (Fig. 3). The sedimentary xenoliths have retained their internal bedding structure. Most display preferred orientation with the long axis parallel to the dyke margin as well as textures typical of plastic-deformation environments including boudinage and pinching. Clasts have also been fractured and cross-cut by the carbonatite.
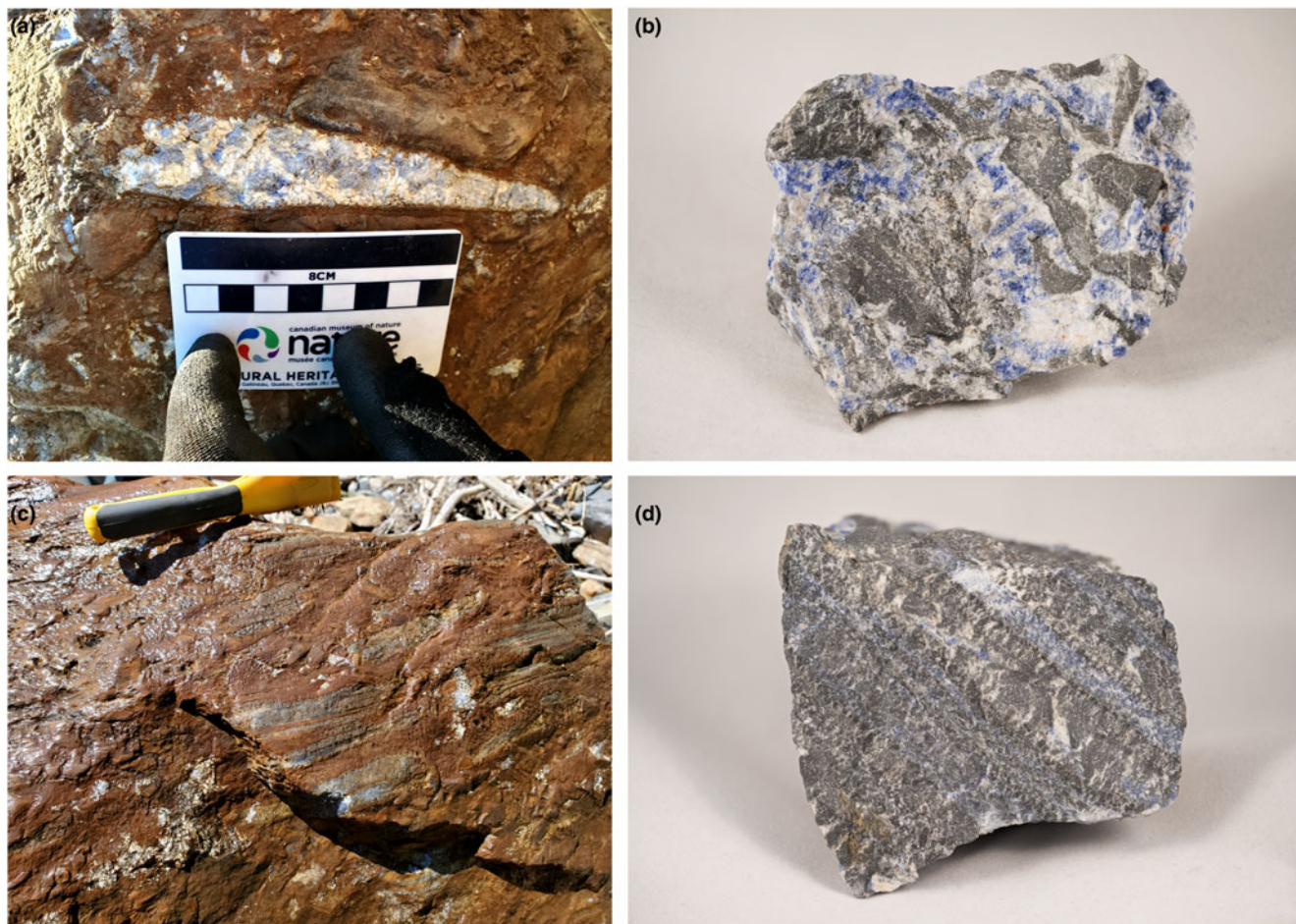
Fig. 3. (a) Sodalite syenite composed of sodalite, microcline, ferroan dolomite and calcite in the breccia groundmass. (b) Carbonate-rich sodalite syenite with host-rock clasts. Sample is 8.5 × 5.8 cm. (c) Bands of fine-grained sodalite and carbonates in the breccia groundmass. The yellow brush for scale is 20 cm long. (d) Bands of fine-grained sodalite and carbonate showing the pervasive blue colouration. Sample is 7.3 × 5.6 cm.

The sodalite-carbonate segregations consist dominantly of sodalite, ferroan dolomite, calcite and microcline, with an extensive suite of trace minerals enriched in REE, Na, Ba and Sr, including albite, analcime, ancylite-(Ce), chabazite-Na, fluorapatite, baryte, barytocalcite, cancrinite, galena, goethite, gonnardite, harmotome, edingtonite, a potentially new Mg-bearing edingtonite-like mineral, natrolite, nordstrandite, pyrite, quintinite and sphalerite (Fig. 4).

Mineral compositions

Quantitative compositions of the Mount Mather Creek minerals were determined using a JEOL SuperProbe 8230 electron probe microanalyser (EPMA) operating in wavelength-dispersive mode using *Probe for EPMA Extreme Edition* software at the University of Ottawa. Analytical conditions for the various minerals are reported in Supplementary Table S1.

Time-dependant intensities were obtained for volatiles and other beam-sensitive elements in order to assess and correct for ion migration under the beam. Excess F observed in some fluorapatite analyses (>1 atoms per formula unit (apfu)) is possibly due to F migration into the interaction volume, an artefact observed when apatite grains are mounted and analysed in a specific crystallographic orientation (Stormer *et al.*, 1993). To

mitigate this ion migration as much as possible, volatiles in fluorapatite were analysed at a lower current than the other elements (10 nA *versus* 20 nA).

Raw intensities were converted to concentrations using the default φρZ corrections of the *Probe for EPMA* software package (Armstrong, 1988). Elemental interferences were corrected using empirical overlap corrections. Full EPMA for all minerals can be found in Tables 1–8. Contents for H_2O and CO_2 were calculated by difference. All rare earth element (REE) concentrations were normalised to C1 chondrite abundances (McDonough and Sun, 1995).

Powder X-ray diffraction

Powder X-ray diffraction (PXRD) data were collected using a Bruker D8 discover-MR A25 equipped with Dectris Eiger2 R 500K detector. The instrument uses an Incoatec Cu microfocus source (IμS) operating at 50 kV and 1 mA. The sample is mounted on a 250 μm spherical powder pin. A statistical approach (Rowe, 2009) is used to calibrate the image correction parameters (sample-to-detector distance and X-Y beam centre coordinates). Further data correction is achieved with a residual error correction curve obtained with an NBS Si 640a standard and tested with an annealed fluorite standard. The resulting 2θ

			Stage of formation			
	Abbreviation	Formula	Host Rock	1 Groundmass	2 Early carbohydrothermal	3 Late carbo-hydrothermal/ post-magmatic
Carbonates						
Ancylite-(Ce)	Anc-Ce	$SrCe(CO_3)_2(OH) \cdot H_2O$				
Barytocalcite	Bcal	$BaCa(CO_3)_2$				
Calcite	Cal	$Ca(CO_3)$				
Ferroan dolomite	Fe-Dol	$Ca(Mg,Fe)(CO_3)_2$				
Silicates						
Albite	Ab	$Na(AlSi_3O_8)$				
Microcline	Mcc	$K(AlSi_3O_8)$				
Sodalite	Sdl	$Na_4(Si_3Al_3)O_{12}Cl$				
Analcime	Anl	$Na(AlSi_2O_6) \cdot H_2O$				
Edingtonite	Edi	$Ba(Si_3Al_2)O_{10} \cdot 4H_2O$				
Cancrinite	Ccn	$(Na,Ca,\square)_8(Al_6Si_6O_{24})(CO_3,SO_4)_2 \cdot 2H_2O$				
Gonnardite	Gon	$(Na,Ca)_2(Si,Al)_5O_{10} \cdot 3H_2O$				
Chabazite-Na	Cbz	$(Na_3K)[Al_4Si_8O_{24}] \cdot 11H_2O$				
Natrolite	Ntr	$Na_2(Si_3Al_2)O_{10} \cdot 2H_2O$				
Harmotome	Hrm	$Ba_2(Si_{12}Al_4)O_{32} \cdot 12H_2O$				
Hydroxides						
Goethite	Gt	$\alpha\text{-}Fe^{3+}O(OH)$				
Quintinite	Qtn	$Mg_4Al_2(OH)_{12}CO_3 \cdot 3H_2O$				
Nordstrandite	Nsd	$Al(OH)_3$				
Phosphates						
Fluorapatite	Fap	$Ca_5(PO_4)_3F$				
Sulfates						
Baryte	Brt	$Ba(SO_4)$				
Sulfides						
Galena	Gn	PbS				
Pyrite	Py	FeS_2				
Sphalerite	Sp	ZnS				

Fig. 4. Formulae and paragenesis of the minerals at Mount Mather Creek. Abbreviations are according to Warr (2021).

correction curve is applied to an XY data file (with a 0.005° step size) of the diffractogram to fix the instrumentation error, which results in a 2θ error of below +/− 0.001° for the whole diffraction pattern for diffraction peaks and features. Sample exposure time during data collection was 300 s over a range of 70°2θ.

Cathodoluminescence spectroscopy

Cathodoluminescence (CL) and back-scattered electron (BSE) imaging of polished thin sections was undertaken using a JEOL 6610Lv scanning electron microscope equipped with a mono-chromatic Gatan miniCL detector with operating conditions of 15 kV and a beam current of ~1 nA. Additional CL imaging was undertaken using a cold cathode CITL cathodoluminescence MK5 with a CRI Nuance Multispectral Imaging System FX.

Mineralogy

The modal mineralogy of the dyke is heterogeneous and changes on a centimetre scale. Estimates of mineral contents by volume are difficult to determine although total carbonate contents (calcite + ferroan dolomite) range from 40 vol.% in the main dyke to 85 vol.% total carbonates in the small veins. With >50 vol.%

carbonate minerals by volume, the breccia itself can be classified on a non-genetic basis as a carbonatite (Le Maitre, 2002), however it is more appropriately described as a carbohydrothermal breccia (Zaitsev, 1996; Mitchell, 2005).

Four late-stage LREE–Ba–Sr minerals, ancylite-(Ce), baryte, barytocalcite and edingtonite, have been found within the Mount Mather Creek breccia. Of note is the absence of many characteristic *bona fide* carbonatite minerals, including Nb–Ta oxides, REE-fluorocarbonates, magnetite, monazite, or ilmenite. A list of all the identified minerals and their parageneses can be found in Fig. 4.

Major minerals

Ferroan dolomite

Carbonatites are commonly named on the basis of their dominant carbonate mineral (i.e. calcite carbonatite, dolomite carbonatite and ankerite/siderite carbonatite). Ferroan dolomite (see below) is the main carbonate mineral at Mount Mather Creek. It occurs as medium- to coarse-grained (50 μm–2 mm), white to slightly yellow–brown, anhedral grains interstitial to sodalite and micro-cline and intergrown with calcite. In some cases, calcite stringers are present within dolomite, indicating the presence of a second

Table 1. Representative compositions of microcline from Mount Mather Creek.

Sample	01/01/2021				02/01/2021						01/03/2021				02/04/2021			All data (N = 17)		
Wt.%	1	2	3	4	1	2	3	4	5	6	1	2	3	4	1	2	3	Ave.	Min	Max
SiO_2	63.45	64.59	63.77	63.59	63.95	64.36	64.54	64.26	63.74	64.03	64.06	64.05	63.83	63.37	64.00	64.06	63.93	63.98	63.37	64.59
Al_2O_3	18.27	18.51	18.17	18.29	18.27	18.42	18.47	18.34	18.25	18.37	18.34	18.33	18.25	18.61	18.22	18.38	18.28	18.34	18.17	18.61
FeO	0.04	0.03	0.02	0.01	0.02	n.d.	0.00	0.04	0.01	n.d.	0.01	0.03	0.03	0.01	n.d.	0.03	0.01	0.02	n.d.	0.04
MnO	0.03	n.d.	n.d.	0.01	0.01	n.d.	0.01	0.00	0.02	n.d.	0.01	0.01	0.01	0.00	0.01	0.06	0.00	0.01	n.d.	0.06
MgO	0.01	n.d.	0.01	0.01	n.d.	n.d.	0.01	n.d.	n.d.	0.01	0.02	n.d.	n.d.	n.d.	n.d.	0.01	0.01	0.00	n.d.	0.02
CaO	0.01	n.d.	0.03	0.02	0.03	0.03	0.06	0.09	0.02	0.01	0.02	n.d.	0.06	0.09	n.d.	0.03	0.06	0.03	n.d.	0.09
BaO	0.07	0.13	0.10	0.21	0.19	0.17	0.19	0.08	0.11	0.14	0.17	0.12	0.15	0.20	0.08	0.07	0.16	0.14	0.07	0.21
Na_2O	0.24	0.22	0.26	0.22	0.24	0.25	0.28	0.25	0.21	0.21	0.21	0.22	0.35	0.25	0.20	0.30	0.27	0.25	0.20	0.35
K_2O	16.18	16.66	16.49	16.40	16.93	16.68	16.70	16.49	16.43	16.69	16.97	16.30	16.55	15.89	16.47	16.60	16.36	16.52	15.89	16.97
Total	99.14	100.14	98.91	99.18	99.66	99.92	100.28	99.63	98.87	99.45	99.82	99.11	99.28	98.51	99.00	99.55	99.11	99.39	98.51	100.28
Formulae based on 8 oxygens pfu																				
Na	0.022	0.020	0.024	0.020	0.021	0.022	0.025	0.023	0.019	0.019	0.019	0.020	0.032	0.023	0.018	0.027	0.024	0.022	0.018	0.032
K	0.969	0.984	0.988	0.981	1.008	0.988	0.986	0.979	0.984	0.993	1.009	0.972	0.989	0.953	0.983	0.987	0.976	0.984	0.953	1.009
Ca	0.001	0.000	0.002	0.001	0.002	0.002	0.003	0.004	0.001	0.001	0.001	n.d.	0.003	0.004	0.000	0.002	0.003	0.002	n.d.	0.004
Ba	0.001	0.002	0.002	0.004	0.003	0.003	0.003	0.002	0.002	0.002	0.003	0.002	0.003	0.004	0.001	0.001	0.003	0.003	0.001	0.004
Fe^{2+}	0.001	0.001	0.001	n.d.	0.001	n.d.	n.d.	0.002	0.001	n.d.	n.d.	0.001	n.d.	n.d.	n.d.	0.002	n.d.	0.001	n.d.	0.002
Mn	0.001	n.d.	n.d.	n.d.	n.d.	n.d.	0.001	n.d.	n.d.	n.d.	n.d.	n.d.	n.d.	n.d.	n.d.	n.d.	n.d.	n.d.	n.d.	0.001
Mg	0.001	n.d.	0.001	n.d.	0.001	n.d.	n.d.	n.d.	n.d.	n.d.	n.d.	n.d.	n.d.	0.001	n.d.	n.d.	0.001	n.d.	n.d.	0.001
Si	2.978	2.990	2.994	2.982	2.985	2.989	2.987	2.991	2.993	2.988	2.986	2.993	2.989	2.980	2.995	2.986	2.990	2.988	2.978	2.995
Al	1.011	1.010	1.005	1.011	1.005	1.008	1.007	1.006	1.010	1.010	1.008	1.010	1.007	1.031	1.005	1.010	1.008	1.010	1.005	1.031
Ab	2.17	1.95	2.37	1.99	2.07	2.22	2.47	2.27	1.88	1.88	1.84	1.98	3.13	2.34	1.84	2.70	2.40	2.21	1.84	3.13
An	0.06	0.00	0.15	0.11	0.15	0.17	0.30	0.42	0.09	0.05	0.09	0.00	0.28	0.45	0.00	0.16	0.30	0.16	0.00	0.45
Or	97.77	98.04	97.47	97.90	97.78	97.61	97.23	97.30	98.03	98.06	98.07	98.02	96.59	97.21	98.16	97.13	97.30	97.63	96.59	98.16

n.d. – not detected

generation of calcite. In carbonate-dominant veins, ferroan dolomite and calcite form in a syngenetic comb texture, with prismatic crystals up to 2.5 mm, bordered frequently by subhedral sodalite at the contact with the host-rock clasts (Fig. 5).

At Mount Mather Creek, the main carbonate mineral contains 8.66–11.16 wt.% FeO, corresponding to Fe = 0.23–0.34 apfu with an Mg/[Mg+Fe] ratio ranging from 0.64 to 0.76 (av. 0.68). Only minor compositional variation is observed within and between grains. The Mn contents range from 0.03 to 0.06 apfu (1.02–2.05 wt.% MnO), higher than that observed in coeval calcite (Mn = 0.002–0.01 apfu), and Sr is at or below the detection limit. The average composition is $Ca_{1.010}(Mg_{0.653}Fe_{0.304}Mn_{0.041})_{\Sigma 1.000}(CO_3)_2$ (Fig. 6).

In this work we use the term ferroan dolomite rather than ankerite to describe the Fe–Mg-bearing carbonates. The use and definition of the term 'ankerite' is commonly used loosely by authors to describe any Fe-rich dolomite, regardless of the Fe/Mg ratio. However, the definition of 'ankerite' remains imprecise and has been used for Ca–Fe–Mg carbonates containing >10% $FeCO_3$ (Hey, 1950), >18 wt.% FeO (Chakhmouradian et al., 2016) and Mg/(Mg+Fe) <0.8 (Chang et al., 1996). The situation is complicated the fact that members along this join, especially from carbonatites, typically have substantial Mn and Zn, resulting in deviation from the dolomite–ankerite join.

Strictly speaking, ankerite, $CaFe(CO_3)_2$, is the ordered Fe end-member in the solid solution series with dolomite, $CaMg(CO_3)_2$. Using the IMA's 50% rule (Nickel and Grice, 1998; Hatert and Burke, 2008), ankerite is any mineral in the $Ca(Mg,Fe,Mn)(CO_3)_2$ series with Fe >50% or the predominant cation of that site. Although compositions with up to 70 mol.% $CaFe(CO_3)_2$ occur in nature, end-member, ordered ankerite has not been found, nor has it been synthesised (Reeder and Dollase, 1989; Chai and Navrotsky, 1996; Chakhmouradian et al., 2016). Above 70 mol.% $CaFe(CO_3)_2$ and at temperatures >350°C, ankerite lies in a two-phase field consisting of disordered siderite and calcite (Rosenberg, 1967, 1968). Chai and Navrotsky (1996) demonstrated that, relative to a two-phase mixture of siderite and calcite, end-member $CaFe(CO_3)_2$ is energetically and structurally unstable. They suggest that although possible at low temperatures, kinetic barriers prevent an ordered stacking of Fe and Ca layers and that ordered ankerite in nature is non-existent. The presence of Mn or Zn further decreases its stability.

Calcite

Calcite occurs in four different textures and associations: (1) early groundmass calcite intergrown with ferroan dolomite, sodalite and microcline; (2) veins of prismatic crystals up to 2.5 mm in length intergrown with ferroan dolomite in a comb texture (Fig. 5); (3) in bands with fine-grained sodalite and ferroan dolomite (Fig. 7); (4) as a late-stage overgrowth in vugs and along fractures in sodalite, microcline and ferroan dolomite (Fig. 8); and (5) replacing barytocalcite together with baryte (Fig. 9). The early matrix calcite occurs as fine- to coarse-grained, anhedral-to-subhedral, colourless grains with ferroan dolomite, interstitial to sodalite and microcline. In the syenite, the calcite is fine grained (0.06–0.3 mm) and granular, interstitial to the sodalite and microcline, and in places has undergone partial recrystallisation as evidenced by the presence of patchy, Sr-rich zones. Calcite grain size increases with distance from the microcline-rich syenitic segregations into the main breccia groundmass where it becomes anhedral-to-subhedral and medium grained. The transition from sodalite syenite into the

Table 2. Representative compositions of sodalite from Mount Mather Creek.

Sample Wt.%	2021–1–1			2021–1–2				2021–3–1		2021–4–1				2021–4–2				All data ($N = 17$)		
	1	2	3	1	2	3	4	1	2	1	2	3	4	1	2	3	4	Ave.	Min.	Max.
SiO_2	37.16	37.41	37.13	37.54	37.27	36.79	37.07	36.75	37.38	36.50	36.70	36.52	36.80	36.93	38.24	37.13	37.07	37.08	36.50	38.24
TiO_2	0.01	n.d.	0.01	n.d.	n.d.	n.d.	0.01	n.d.	n.d.	0.02	0.01	0.01	0.01	n.d.	n.d.	n.d.	0.02	0.01	n.d.	0.02
Al_2O_3	31.82	31.73	31.56	31.88	31.71	31.47	31.63	31.74	31.86	31.55	31.76	31.69	31.80	31.72	32.23	31.80	32.24	31.77	31.47	32.24
FeO	n.d.	0.01	0.03	0.01	0.02	0.02	n.d.	n.d.	0.03	n.d.	0.03	0.01	0.03	n.d.	n.d.	n.d.	n.d.	0.01	n.d.	0.03
MnO	n.d.	n.d.	0.01	n.d.	n.d.	n.d.	n.d.	n.d.	n.d.	n.d.	0.01	n.d.	0.02	0.01	0.02	0.01	0.01	0.01	n.d.	0.02
MgO	n.d.	n.d.	n.d.	n.d.	n.d.	n.d.	n.d.	n.d.	n.d.	n.d.	n.d.	n.d.	0.02	n.d.	n.d.	n.d.	n.d.	n.d.	n.d.	0.02
CaO	0.01	0.06	0.02	0.11	0.04	0.16	0.10	0.02	0.01	0.01	0.02	0.05	0.06	n.d.	0.01	0.02	0.02	0.04	n.d.	0.16
Na_2O	25.91	26.03	26.20	25.52	25.73	25.94	25.70	26.41	25.85	25.78	25.99	26.22	25.88	26.50	26.12	25.80	25.35	25.94	25.35	26.50
K_2O	0.02	0.03	0.02	0.03	0.03	0.04	0.04	0.03	0.02	0.02	0.04	0.04	0.04	0.03	0.04	0.03	0.06	0.03	0.02	0.06
SO_3^-	n.d.	0.01	0.03	0.01	0.04	0.03	n.d.	n.d.	0.02	n.d.	0.02	0.03	n.d.	n.d.	n.d.	n.d.	n.d.	0.01	n.d.	0.04
Cl^-	7.53	7.19	7.19	7.08	7.27	7.08	7.28	7.29	7.18	7.29	7.27	7.27	7.62	7.28	7.25	7.26	6.93	7.25	6.93	7.62
F^-	n.d.	n.d.	n.d.	n.d.	0.05	0.18	0.05	n.d.	n.d.	n.d.	n.d.	0.02	0.04	n.d.	n.d.	n.d.	n.d.	0.02	n.d.	0.18
O=Cl,F	–1.70	–1.62	–1.62	–1.60	–1.66	–1.67	–1.66	–1.64	–1.62	–1.64	–1.64	–1.65	–1.73	–1.64	–1.64	–1.64	–1.56	–1.64	–1.73	–1.56
Total	100.77	100.86	100.57	100.58	100.50	100.04	100.22	100.60	100.71	99.52	100.20	100.20	100.58	100.82	102.28	100.42	100.15	100.53	99.52	102.28
Formulae based on 12 oxygens pfu																				
Na	4.037	4.033	4.077	3.949	4.005	4.067	4.016	4.122	4.005	4.062	4.066	4.110	4.054	4.124	3.980	4.018	3.934	4.039	3.934	4.124
K	0.002	0.003	0.002	0.003	0.003	0.004	0.004	0.004	0.002	0.002	0.004	0.005	0.004	0.003	0.004	0.003	0.006	0.003	0.002	0.006
Ca	0.001	0.005	0.001	0.009	0.004	0.014	0.009	0.001	0.001	0.001	0.002	0.004	0.005	n.d.	n.d.	0.002	0.002	0.004	n.d.	0.014
Fe^{2+}	n.d.	0.001	0.002	n.d.	0.001	0.001	n.d.	n.d.	0.002	n.d.	0.002	0.001	0.002	n.d.	n.d.	n.d.	n.d.	0.001	n.d.	0.002
Mn	n.d.	n.d.	0.001	n.d.	n.d.	n.d.	n.d.	n.d.	n.d.	n.d.	0.001	n.d.	0.001	0.001	0.001	0.001	0.001	n.d.	n.d.	0.001
Mg	n.d.	n.d.	n.d.	n.d.	n.d.	n.d.	n.d.	0.001	n.d.	n.d.	n.d.	n.d.	0.002	n.d.	n.d.	n.d.	n.d.	n.d.	n.d.	0.002
Al	3.013	2.988	2.986	2.998	3.000	3.000	3.005	3.011	3.001	3.022	3.020	3.019	3.027	3.001	2.986	3.010	3.041	3.008	2.986	3.041
Si	2.986	2.989	2.980	2.996	2.993	2.976	2.988	2.958	2.988	2.966	2.961	2.952	2.972	2.964	3.005	2.983	2.966	2.978	2.952	3.005
Ti	0.001	n.d.	0.001	n.d.	n.d.	n.d.	0.001	n.d.	n.d.	0.001	0.001	0.001	0.001	n.d.	n.d.	n.d.	0.001	n.d.	n.d.	0.001
Cl	1.026	0.973	0.979	0.957	0.990	0.970	0.995	0.994	0.972	1.004	0.994	0.996	1.043	0.990	0.966	0.988	0.940	0.987	0.940	1.043
F	n.d.	n.d.	n.d.	n.d.	0.013	0.045	0.013	n.d.	n.d.	n.d.	n.d.	0.004	0.010	n.d.	n.d.	n.d.	n.d.	0.005	n.d.	0.045
SO_4^{2-}	n.d.	0.001	0.002	0.001	0.002	0.002	n.d.	n.d.	0.001	n.d.	0.001	0.002	n.d.	n.d.	n.d.	n.d.	n.d.	0.001	n.d.	0.002

n.d. – not detected

Table 3. Representative compositions of ancylite-(Ce) from Mount Mather Creek.

Wt.%	1	2	3	4	5	6	7	8	9	10	11	12	13	14	15	Ave.[1]	Min	Max
SiO_2	0.13	0.06	0.02	0.25	n.d.	0.01	0.01	0.04	n.d.	n.d.	0.01	n.d.	0.03	0.08	0.31	0.06	n.d.	0.31
PbO	n.d.	n.d.	n.d.	n.d.	n.d.	0.04	n.d.	n.d.	n.d.	0.08	n.d.	n.d.	n.d.	n.d.	n.d.	0.01	n.d.	0.08
ThO_2	1.72	1.61	1.68	1.05	1.63	1.81	1.33	2.25	1.96	1.93	2.00	1.36	1.24	2.24	2.10	1.73	1.05	2.25
Y_2O_3	0.17	0.17	0.20	0.13	0.17	0.11	0.11	0.04	0.10	0.10	0.16	0.11	0.08	0.44	0.42	0.17	0.04	0.44
La_2O_3	13.41	11.70	12.00	10.44	11.19	11.61	10.65	12.75	11.49	14.76	14.26	11.97	12.42	9.80	9.67	11.87	9.67	14.76
Ce_2O_3	21.32	21.14	21.18	20.34	20.63	20.07	19.26	21.13	19.80	20.74	20.39	21.95	20.25	21.42	20.89	20.70	19.26	21.95
Pr_2O_3	2.22	2.47	2.19	2.12	2.26	1.87	2.13	2.01	2.22	1.77	1.83	2.42	1.89	2.54	2.37	2.15	1.77	2.54
Nd_2O_3	8.34	9.80	9.11	9.24	8.50	7.98	8.48	7.17	7.78	6.32	6.06	9.52	6.76	9.44	9.58	8.27	6.06	9.80
Sm_2O_3	1.35	1.53	1.45	1.20	1.03	0.88	0.96	0.83	0.72	0.73	0.84	1.07	0.63	1.48	1.34	1.07	0.63	1.53
Eu_2O_3	0.45	0.43	0.48	0.35	0.21	0.22	0.19	0.21	0.11	0.19	0.12	0.39	0.08	0.08	0.59	0.45	0.08	0.59
FeO	n.d.	n.d.	n.d.	0.03	n.d.	n.d.	n.d.	n.d.	n.d.	n.d.	0.02	n.d.	n.d.	0.04	n.d.	0.01	n.d.	0.04
MnO	n.d.	n.d.	0.02	0.02	0.04	0.05	0.05	0.04	0.02	n.d.	0.02	n.d.	n.d.	0.03	n.d.	0.02	n.d.	0.05
MgO	n.d.	n.d.	n.d.	n.d.	n.d.	n.d.	n.d.	n.d.	n.d.	n.d.	n.d.	n.d.	n.d.	n.d.	0.04	n.d.	n.d.	0.04
CaO	2.25	2.23	2.33	2.76	2.94	2.11	2.09	2.49	2.11	2.22	2.06	1.73	2.20	3.34	3.30	2.41	1.73	3.34
SrO	19.66	18.30	19.98	20.79	20.96	23.49	23.02	22.30	24.45	20.95	22.31	20.66	23.73	16.92	17.49	21.00	16.92	24.45
BaO	0.50	0.26	0.31	1.08	1.03	0.35	0.27	0.33	0.31	0.06	n.d.	n.d.	0.54	0.55	0.34	0.40	n.d.	1.08
Na_2O	n.d.	n.d.	n.d.	0.01	n.d.	n.d.	n.d.	n.d.	n.d.	n.d.	n.d.	n.d.	n.d.	n.d.	0.07	0.05	0.01	n.d.	0.07
F	1.04	0.85	0.92	0.65	0.74	1.15	1.11	1.20	1.21	1.21	1.16	0.82	1.19	n.d	0.04	0.89	n.d.	1.21
CO_2	23.27	22.52	23.16	23.41	23.56	23.51	22.92	23.75	23.76	22.94	23.16	23.03	23.46	22.77	22.77	23.20	22.52	23.76
H_2O	6.65	6.51	6.68	6.88	6.88	6.67	6.51	6.72	6.72	6.47	6.56	6.68	6.64	6.99	6.97	6.70	6.47	6.99
$O=F_2$	−0.44	−0.36	−0.39	−0.27	−0.31	−0.48	−0.47	−0.51	−0.51	−0.51	−0.49	−0.35	−0.50	n.d.	−0.02	−0.37	−0.51	0.00
Total	102.05	99.23	101.32	100.48	101.46	101.44	98.62	102.76	102.26	99.96	100.47	101.36	100.63	98.74	98.12	100.59	98.12	102.76
Formulae based on 2 cations pfu, with OH+F = 1 apfu and CO_3 = 2 apfu																		
Sr	0.718	0.690	0.733	0.754	0.756	0.849	0.853	0.798	0.874	0.776	0.818	0.762	0.859	0.631	0.652	0.768	0.631	0.874
Ba	0.012	0.007	0.008	0.026	0.025	0.009	0.007	0.008	0.007	0.002	n.d.	n.d.	0.013	0.014	0.009	0.010	n.d.	0.026
Ca	0.152	0.155	0.158	0.185	0.196	0.141	0.143	0.165	0.139	0.152	0.140	0.118	0.147	0.230	0.227	0.163	0.118	0.230
Pb	n.d.	n.d.	n.d.	n.d.	n.d.	0.001	n.d.	n.d.	n.d.	0.001	n.d.	n.d.	n.d.	n.d.	n.d.	n.d.	n.d.	0.001
Fe^{2+}	n.d.	n.d.	n.d.	0.002	n.d.	n.d.	n.d.	n.d.	n.d.	n.d.	0.001	n.d.	n.d.	0.002	n.d.	n.d.	n.d.	0.002
Mn	n.d.	n.d.	0.001	0.001	0.002	0.003	0.003	0.002	0.001	n.d.	0.001	n.d.	n.d.	0.002	n.d.	0.001	n.d.	0.003
Mg	n.d.	n.d.	n.d.	n.d.	n.d.	n.d.	n.d.	n.d.	n.d.	n.d.	n.d.	n.d.	n.d.	n.d.	0.004	n.d.	n.d.	0.004
Na	n.d.	n.d.	n.d.	0.001	n.d.	n.d.	n.d.	n.d.	n.d.	n.d.	0.000	n.d.	n.d.	0.009	0.006	0.001	n.d.	0.009
Si	0.008	0.004	0.001	0.016	n.d.	0.001	0.001	0.002	n.d.	n.d.	0.001	n.d.	0.002	0.005	0.020	0.004	n.d.	0.020
Th	0.025	0.024	0.024	0.015	0.023	0.026	0.019	0.032	0.027	0.028	0.029	0.020	0.018	0.033	0.031	0.025	0.015	0.033
Sum	0.915	0.880	0.925	1.000	1.002	1.030	1.026	1.007	1.048	0.959	0.990	0.900	1.039	0.926	0.949	0.973	0.880	1.048
La	0.311	0.281	0.280	0.241	0.257	0.267	0.251	0.290	0.261	0.348	0.333	0.281	0.286	0.233	0.229	0.277	0.229	0.348
Ce	0.491	0.503	0.490	0.466	0.470	0.458	0.451	0.477	0.447	0.485	0.472	0.511	0.463	0.504	0.492	0.479	0.447	0.511
Pr	0.051	0.059	0.050	0.048	0.051	0.042	0.050	0.045	0.050	0.041	0.042	0.056	0.043	0.060	0.056	0.050	0.041	0.060
Nd	0.187	0.228	0.206	0.207	0.189	0.178	0.194	0.158	0.171	0.144	0.137	0.216	0.151	0.217	0.220	0.187	0.137	0.228
Sm	0.029	0.034	0.032	0.026	0.022	0.019	0.021	0.018	0.015	0.016	0.018	0.023	0.014	0.033	0.030	0.023	0.014	0.034
Eu	0.010	0.010	0.010	0.007	0.004	0.005	0.004	0.004	0.002	0.004	0.003	0.008	0.002	0.013	0.010	0.006	0.002	0.013
Y	0.006	0.006	0.007	0.004	0.006	0.004	0.004	0.001	0.003	0.003	0.005	0.004	0.003	0.015	0.014	0.006	0.001	0.015
Sum	1.085	1.121	1.075	0.999	0.999	0.973	0.975	0.993	0.949	1.041	1.010	1.099	0.962	1.075	1.051	1.027	0.949	1.121
F^-	0.207	0.175	0.184	0.129	0.146	0.227	0.224	0.234	0.236	0.244	0.232	0.165	0.235	n.d.	0.008	0.176	n.d.	0.244
OH^-	0.793	0.825	0.816	0.871	0.854	0.773	0.776	0.766	0.764	0.756	0.768	0.835	0.765	1.000	0.992	0.824	0.756	1.000
CO_3	2.000	2.000	2.000	2.000	2.000	2.000	2.000	2.000	2.000	2.000	2.000	2.000	2.000	2.000	2.000	2.000	2.000	2.000

[1]N = 15; n.d. – not detected

Table 4. Representative compositions of barytocalcite from Mount Mather Creek.

Wt. %	1	2	3	4	5	6	7	8	9	10	11	12
ThO_2	n.d.	n.d.	n.d.	n.d.	n.d.	n.d.	0.05	n.d.	0.14	0.04	n.d.	0.06
Ce_2O_3	0.18	0.34	n.d.	n.d.	0.19	0.08	0.20	0.21	n.d.	0.08	n.d.	0.19
FeO	0.02	0.02	n.d.	0.08	n.d.	0.04	n.d.	0.10	0.08	n.d.	n.d.	n.d.
CaO	18.52	18.31	18.60	18.55	18.47	18.77	18.63	19.00	18.37	19.00	18.75	18.72
SrO	0.06	n.d.	0.08	0.02	n.d.	0.05	0.04	0.15	0.10	0.10	0.05	0.19
BaO	52.75	52.61	52.51	52.54	52.54	52.73	52.58	52.53	52.41	52.77	52.98	52.11
Na_2O	0.06	0.05	0.08	0.09	0.06	0.07	0.07	0.07	0.15	0.09	0.06	0.12
CO_2	29.10	29.09	29.20	29.21	29.12	29.07	29.13	29.11	29.19	29.07	29.04	29.23
Total	100.72	100.66	100.56	100.51	100.61	101.00	100.76	101.18	100.53	101.20	101.05	100.69
Formula based on 6 oxygens pfu												
Ba	1.032	1.030	1.025	1.026	1.032	1.032	1.027	1.022	1.024	1.028	1.035	1.015
Sr	0.002	n.d.	0.002	0.001	n.d.	0.002	0.001	0.004	0.003	0.003	0.002	0.006
Ca	0.991	0.980	0.993	0.990	0.988	1.002	0.995	1.011	0.982	1.013	1.002	0.997
Na	0.005	0.005	0.008	0.009	0.006	0.007	0.007	0.007	0.006	0.014	0.008	0.006	0.011
Fe^{2+}	0.001	0.001	n.d.	0.003	n.d.	0.002	n.d.	0.004	0.003	n.d.	n.d.	n.d.
Ce	0.003	0.006	0.001	n.d.	0.004	0.001	0.004	0.004	0.001	0.001	n.d.	0.003
Eu	n.d.	0.001	0.001	n.d.	n.d.	n.d.	n.d.	n.d.	n.d.	0.001	0.001	0.001
Th	n.d.	n.d.	n.d.	n.d.	n.d.	n.d.	0.001	n.d.	0.002	n.d.	n.d.	0.001
C	1.983	1.985	1.987	1.987	1.985	1.978	1.983	1.974	1.987	1.974	1.977	1.984

Wt. %	13	14	15	16	17	18	19	20	21	Ave. [1]	Min	Max
ThO_2	0.01	n.d.	n.d.	n.d.	n.d.	0.05	n.d.	n.d.	n.d.	n.d.	n.d.	0.14
Ce_2O_3	n.d.	n.d.	0.11	n.d.	n.d.	n.d.	n.d.	n.d.	n.d.	0.08	n.d.	0.34
FeO	0.02	0.03	n.d.	n.d.	n.d.	n.d.	0.01	n.d.	0.03	0.02	n.d.	0.10
CaO	18.78	18.89	18.71	19.07	18.60	18.61	18.48	18.61	18.59	18.67	18.31	19.07
SrO	0.09	0.04	0.08	0.08	0.14	0.05	0.08	0.12	0.10	0.08	n.d.	0.19
BaO	52.48	52.81	52.89	53.29	53.18	49.40	52.44	52.86	52.74	52.54	49.40	53.29
Na_2O	0.07	0.12	0.07	0.10	0.09	0.11	0.10	0.08	0.06	0.08	0.05	0.15
CO_2	29.20	29.11	29.07	28.92	28.99	30.17	29.23	29.07	29.15	29.17	28.92	30.17
Total	100.71	101.01	100.95	101.61	101.03	98.51	100.45	100.88	100.65	100.73	98.51	101.61
Formula based on 6 oxygens pfu												
Ba	1.023	1.030	1.033	1.040	1.041	0.953	1.024	1.034	1.031	1.026	0.953	1.041
Sr	0.003	0.001	0.002	0.002	0.004	0.001	0.002	0.004	0.003	0.002	n.d.	0.006
Ca	1.001	1.007	1.000	1.017	0.996	0.982	0.987	0.995	0.993	0.996	0.980	1.017
Na	0.007	0.012	0.007	0.010	0.009	0.010	0.010	0.008	0.006	0.008	0.005	0.014
Fe^{2+}	0.001	0.001	n.d.	n.d.	n.d.	n.d.	n.d.	n.d.	0.001	0.001	n.d.	0.004
Ce	n.d.	n.d.	0.002	0.001	n.d.	n.d.	n.d.	n.d.	n.d.	0.001	n.d.	0.006
Eu	0.001	n.d.	n.d.	0.002	n.d.	n.d.	n.d.	n.d.	n.d.	n.d.	n.d.	0.002
Th	n.d.	0.000	n.d.	n.d.	n.d.	0.001	n.d.	n.d.	n.d.	n.d.	n.d.	0.002
C	1.984	1.978	1.979	1.966	1.977	2.028	1.989	1.980	1.985	1.983	1.966	2.028

[1]$N = 21$; n.d. – not detected

carbonate-dominated groundmass is marked by this change in grain size.

Secondary calcite occurs as fracture-fillings in sodalite and ferroan dolomite, replacing sodalite and earlier calcite and ferroan dolomite, as well as very fine grained, feathery white overgrowths on late-stage vug minerals including quintinite, ancylite-(Ce), analcime and chabazite-Na (Fig. 10).

Calcite in the syenite, the matrix and in the comb-textured veins has a similar composition (Fig. 6) with Fe+Mn contents ranging from 0.013–0.026 apfu (av. 0.021 apfu), Mg = 0.005–0.021 apfu (av. 0.010 apfu) and very low Sr (av. 0.001 apfu/0.16 wt.% SrO). Late-stage fracture- and vug-filling calcite associated with sodalite, ancylite-(Ce), and quintinite is almost pure end-member with Fe + Mn = 0–0.007 apfu, Mg = 0.002–0.008 apfu and no detectable Sr.

Late-stage calcite and baryte are replacement minerals after barytocalcite. The calcite is Sr-rich, with up to 0.041 apfu Sr (4.17 wt.% SrO; Table 1). Replacement textures and compositional zonation patterns are complex (Fig. 10), with Sr-rich areas concentrated along fractures in the sodalite, suggesting infiltration of late-stage fluids enriched in Sr, or remobilisation

of Sr *via* the fluids from earlier phases [i.e. barytocalcite, ancylite-(Ce)].

Microcline

The potassium feldspar, identified as microcline by PXRD, is a primary magmatic phase in the sodalite syenite, occurring as clusters of medium- to coarse-grained, subhedral, blocky-to-tabular white crystals ranging in size from 0.5–4 mm in length and 0.2–1.5 mm in width. The crystals have undergone moderate to extensive sericitisation, and edges adjacent to dolomite or calcite are commonly rounded and embayed, suggesting some degree of dissolution and alteration by late-stage fluids. All microcline exhibits patchy optical zoning, with only remnants of the original textures, supporting the hypothesis of late-stage alteration.

Compositional zoning was not observed in back-scattered electron images (BSEI), however analyses indicate that rims that are adjacent to calcite or dolomite are enriched in the An component (An 0.45–1.17) relative to cores or rims adjacent to sodalite (An 0.0–0.45). The average composition is $Ab_{2.2}An_{0.2}Or_{97.6}$, and thus outside of the Ab–Or solvus (Table 1). The low Ab

Table 5. Representative compositions of edingtonite (Edi) and a potentially new Mg-bearing edingtonite-like mineral (Mg-edi) from Mount Mather Creek.

Wt.%	Edingtonite											Mg-bearing edingtonite-like		
	Edi-1	Edi-2	Edi-3	Edi-4	Edi-5	Edi-6	Edi-7	Edi-8	Ave. ($N=8$)	Min.	Max.	Mg-Edi-1	Mg-Edi-2	Mg-Edi-3
SiO_2	31.61	32.32	33.65	33.47	34.62	34.33	33.76	33.79	33.44	31.61	34.62	30.73	30.53	30.46
TiO_2	0.01	n.d.	n.d.	n.d.	n.d.	n.d.	n.d.	n.d.	n.d.	n.d.	0.01	0.04	0.08	0.08
Al_2O_3	21.47	23.58	23.09	23.13	23.14	23.14	23.03	22.99	22.95	21.47	23.58	24.08	24.37	24.23
FeO	n.d.	n.d.	n.d.	n.d.	0.01	0.01	0.04	0.08	0.02	n.d.	0.08	0.02	0.01	0.03
MnO	n.d.	n.d.	0.04	0.03	0.03	n.d.	n.d.	n.d.	0.01	n.d.	0.04	0.01	0.01	n.d.
MgO	0.18	0.11	0.26	0.13	n.d.	0.12	0.05	0.06	0.11	n.d.	0.26	1.79	1.94	1.94
CaO	0.65	0.44	0.31	0.31	0.17	0.26	0.29	0.20	0.33	0.17	0.65	0.20	0.20	0.20
SrO	1.42	0.42	0.27	0.17	0.10	0.21	0.17	0.14	0.36	0.10	1.42	1.37	1.36	1.42
BaO	29.55	30.83	30.51	30.09	31.38	31.01	30.92	31.65	30.74	29.55	31.65	26.36	26.35	26.11
Na_2O	0.37	0.16	0.29	0.20	0.27	0.36	0.25	0.30	0.28	0.16	0.37	0.13	0.15	0.17
K_2O	0.53	0.61	0.53	0.59	0.69	0.61	0.55	0.58	0.59	0.53	0.69	0.23	0.22	0.23
H_2O (calc)	13.84	14.38	14.60	14.50	14.80	14.77	14.61	14.62	14.52	13.84	14.80	14.22	14.25	14.20
Total	99.63	102.85	103.55	102.62	105.21	104.82	103.67	104.41	103.35	99.63	105.21	99.18	99.47	99.07
14 oxygens pfu												56 oxygens pfu		
Si	2.739	2.696	2.764	2.769	2.805	2.788	2.771	2.773	2.788	2.696	2.805	10.367	10.275	10.292
Al	2.193	2.318	2.235	2.255	2.210	2.215	2.228	2.223	2.219	2.193	2.318	9.574	9.666	9.649
Sum	4.932	5.014	5.000	5.024	5.015	5.003	4.999	4.996	5.007	4.932	5.024	19.941	19.941	19.941
Mg	0.023	0.014	0.032	0.016	n.d.	0.015	0.006	0.007	0.012	n.d.	0.032	0.900	0.973	0.977
Fe^{2+}	n.d.	n.d.	n.d.	n.d.	0.001	0.001	0.003	0.006	0.002	n.d.	0.006	0.006	0.003	0.008
Mn	n.d.	n.d.	0.003	0.002	0.002	n.d.	n.d.	n.d.	0.001	n.d.	0.003	0.003	0.003	n.d.
Ti	0.001	n.d.	0.001	0.002	n.d.	0.002	n.d.	0.005	0.003	n.d.	0.005	0.010	0.020	0.020
Sum	0.025	0.014	0.036	0.020	0.003	0.017	0.009	0.018	0.020	0.003	0.036	0.929	1.006	1.005
Ba	1.004	1.008	0.982	0.976	0.996	0.987	0.995	1.018	0.846	0.976	1.018	3.485	3.475	3.457
Sr	0.071	0.020	0.013	0.008	0.005	0.010	0.008	0.007	0.012	0.005	0.071	0.268	0.265	0.278
Ca	0.060	0.039	0.027	0.028	0.015	0.023	0.026	0.018	0.130	0.015	0.060	0.072	0.072	0.072
Na	0.062	0.026	0.046	0.032	0.043	0.057	0.040	0.048	0.059	0.026	0.062	0.085	0.098	0.111
K	0.059	0.065	0.056	0.062	0.071	0.063	0.058	0.061	0.085	0.056	0.071	0.099	0.094	0.099
Sum	1.256	1.158	1.124	1.106	1.130	1.139	1.125	1.151	1.132	1.106	1.256	4.009	4.004	4.017

Wt.%	Mg-bearing edingtonite-like mineral													
	Mg-Edi-4	Mg-Edi-5	Mg-Edi-6	Mg-Edi-6	Mg-Edi-7	Mg-Edi-8	Mg-Edi-9	Mg-Edi-10	Mg-Edi-11	Mg-Edi-12	Mg-Edi-13	Ave. ($N = 13$)	Min.	Max.
SiO_2	30.27	30.56	30.79	30.12	30.19	31.76	31.85	30.81	30.82	30.66	31.31	30.78	30.12	31.85
TiO_2	0.04	0.04	0.07	0.02	0.04	0.01	n.d.	n.d.	0.03	n.d.	0.01	0.03	n.d.	0.08
Al_2O_3	24.32	24.41	24.22	24.62	24.75	23.47	23.89	23.51	24.79	25.12	24.58	24.31	23.47	25.12
FeO	n.d.	0.03	0.02	0.37	0.36	0.04	n.d.	0.11	0.01	n.d.	n.d.	0.07	n.d.	0.37
MnO	0.05	n.d.	0.02	0.03	n.d.	n.d.	0.09	n.d.	n.d.	0.03	0.01	0.02	n.d.	0.09
MgO	1.96	1.92	1.91	1.81	1.73	1.70	1.70	1.66	1.95	1.95	1.84	1.84	1.66	1.96
CaO	0.21	0.20	0.24	0.35	0.35	0.28	0.22	0.12	0.07	0.08	0.10	0.20	0.07	0.35
SrO	1.37	1.29	1.42	1.45	1.20	1.78	2.30	1.23	1.19	1.14	1.27	1.41	1.14	2.30
BaO	26.28	26.09	25.67	27.93	28.65	25.13	26.09	28.68	27.56	28.08	27.70	26.91	25.13	28.68
Na_2O	0.24	0.19	0.17	0.12	0.16	0.11	0.10	0.12	0.17	0.14	0.18	0.15	0.10	0.24
K_2O	0.19	0.23	0.25	0.18	0.10	0.43	0.41	0.30	0.19	0.26	0.26	0.25	0.10	0.43
H_2O (calc)	14.18	14.25	14.27	14.31	14.39	14.35	14.51	14.17	14.43	14.50	14.50	14.32	14.17	14.51
Total	99.11	99.21	99.05	101.31	101.92	99.06	101.16	100.71	101.21	101.96	101.76	100.30	99.05	101.96
56 oxygens pfu														
Si	10.240	10.290	10.354	10.096	10.067	10.620	10.533	10.432	10.247	10.143	10.358	10.308	10.067	10.620
Al	9.697	9.687	9.599	9.726	9.727	9.249	9.311	9.382	9.714	9.794	9.583	9.597	9.249	9.794
Sum	19.937	19.977	19.953	19.822	19.794	19.869	19.844	19.814	19.961	19.937	19.941	19.905	19.794	19.977
Mg	0.988	0.964	0.958	0.904	0.860	0.847	0.838	0.838	0.967	0.962	0.907	0.920	0.838	0.988
Fe^{2+}	n.d.	0.008	0.006	0.104	0.100	0.011	n.d.	0.031	0.003	0.000	n.d.	0.020	n.d.	0.104
Mn	0.014	n.d.	0.006	0.009	n.d.	n.d.	0.025	n.d.	n.d.	0.008	0.003	0.005	n.d.	0.025
Ti	0.010	0.010	0.018	n.d.	0.012	n.d.	n.d.	n.d.	n.d.	n.d.	0.012	0.008	n.d.	0.020
Sum	1.012	0.982	0.995	1.022	0.982	0.861	0.863	0.869	0.978	0.970	0.924	0.957	0.861	1.022
Ba	3.484	3.443	3.383	3.669	3.744	3.293	3.381	3.805	3.591	3.640	3.591	3.532	3.293	3.805
Sr	0.269	0.252	0.277	0.282	0.232	0.345	0.441	0.241	0.229	0.219	0.244	0.274	0.219	0.441
Ca	0.076	0.072	0.086	0.126	0.125	0.100	0.078	0.044	0.025	0.028	0.035	0.072	0.025	0.126
Na	0.157	0.124	0.111	0.078	0.103	0.071	0.064	0.079	0.110	0.090	0.115	0.100	0.064	0.157
K	0.082	0.099	0.107	0.077	0.043	0.183	0.173	0.130	0.081	0.110	0.110	0.106	0.043	0.183
Sum	4.068	3.990	3.964	4.232	4.247	3.992	4.137	4.299	4.036	4.087	4.095	4.084	3.964	4.299

n.d. – not detected

Table 6. Powder X-ray diffraction patterns for edingtonite and a potentially-new Mg-edingtonite-like mineral.

Edingtonite[1]		Mg–edingtonite–like mineral[2]		
d_{obs}	I_{obs}[3]	hkl	d_{obs}	I_{obs}
6.547	97	001	6.568	95
5.398	39	101	5.924	32
4.789	100	200	5.448	30
4.699	36	111	4.869	100
4.287	21	210	4.744	76
3.584	75	211	4.504	21
3.391	20	220	3.636	28
3.095	28	102	3.460	15
3.034	67	310	3.431	10
3.009	18	221	3.308	11
2.749	64	311	3.199	25
2.660	15	320	3.117	17
2.599	32	212	3.091	30
2.465	9	321	3.072	26
2.286	44	302	2.990	27
2.260	55	330	2.969	58
2.191	39	411	2.895	20
2.143	20	420	2.796	39
2.137	13	331	2.785	68
2.075	6	113	2.625	50
2.064	9	322	2.538	12
1.896	8	412	2.490	10
1.841	12	431	2.310	30
1.8348	8	223	2.140	12
1.8136	10	511	1.9588	29
			1.8136	11

[1]Mount Mather Creek edingtonite, tetragonal, $P–42_1m$, $a = 9.5968(2)$, $b = 6.5365(3)$ Å, $V = 602.01(4)$ Å^3
[2]Potential orthorhombic cell using Bruker Topas peak indexing solution method, $a = 13.8556(5)$, $b = 6.57964(19)$, $c = 13.7236(4)$ Å and $V = 1251.11(7)$ Å^3
[3]Intensities subject to preferred orientation (measured from a single fragment with Phi–rotation)

component of microcline and the absence of primary albite in the syenite segregations is attributed to the high Na and relatively low Si contents of the melt, resulting in the formation of sodalite over albite. No significant trace-element contents were detected.

Sodalite
Sodalite, $Na_4(Si_3Al_3)O_{12}Cl$, occurs in the syenite segregations, disseminated throughout the matrix and in discontinuous, very fine-grained bands which impart a pervasive blue colouration to the entire rock. Mount Mather Creek sodalite does not show fluorescence under long or shortwave UV light but has a strong, bright blue cold cathode cathodoluminescence (Fig. 11a,b) which fades quickly under the beam. In the syenite, sodalite occurs as subhedral-to-euhedral, medium- to coarse-grained crystals (0.1–4 mm, av. 1 mm) which range in colour from colourless to dark sky blue, most commonly royal blue. Euhedral crystals up to 2 mm can be found in rare vugs together with late-stage ancylite-(Ce), chabazite-Na and quintinite. Microcline laths are intersertal to the sodalite which has a turbid appearance and alternatively well-defined and irregular, lobate-to-embayed boundaries with the carbonate minerals. The sodalite is altered to albite or rarely cancrinite at the margins and has fractures filled with later-stage calcite or a potentially-new Mg-bearing edingtonite-like mineral. In CL images, primary oscillatory zoning can be seen in some of the grains, although the majority have a mottled, patchy appearance (Fig. 11c,d). There is no textural evidence to suggest that sodalite at Mount Mather Creek has crystallised at the expense of earlier feldspars or nepheline, as observed at other

carbonatite–syenite localities (Finch, 1991; Drüppel, 2003; Drüppel et al., 2005). Relict nepheline or albite have not been observed. Fluorite-filled fractures, which have been suggested by Finch (1991) to be an indication of nepheline conversion are not present.

Very fine-grained (25 µm to 0.35 mm, av. 100 µm in width), disseminated sodalite occurs in discontinuous bands in the groundmass up to 12 cm in length and 2 cm in width, giving a pervasive blue tint to the rock. This sodalite occurs as anhedral-to-subhedral, rounded grains (av. 100 µm in width) with an anhedral granular texture with calcite and ferroan dolomite.

Similar textures have been observed at the Swartbooisdrif alkaline complex in Namibia where sodalite occurs in syenite fragments, as lenses and layers within carbonatite and ferrocarbonatite breccia dykes, at the contacts between nepheline syenite and carbonatite, and in metasomatic aureoles at the margins with the host anorthosite (Drüppel, 2003; Drüppel et al., 2005). A similar sodalite–ankerite–baryte dyke has also been described from the Ayopaya province, Bolivia (Schultz et al., 2004).

In terms of composition, sodalite from Mount Mather Creek is that of the almost pure end-member with an average formula of $(Na_{4.039}Ca_{0.004}K_{0.003}Fe_{0.001})_{\Sigma4.047}Al_{3.008}Si_{2.978}[Cl_{0.987}F_{0.005}(SO_4)_{0.001}]_{\Sigma0.992}$ (Table 2). The primary oscillatory zoning observed in CL images was not observed in BSEI and not resolved in EPMA. No variation in composition is observed between the fine-grained, disseminated sodalite and the coarser-grained material in the syenite.

Minor/trace minerals

Albite
Albite is a trace phase (1 vol.%) in the syenite and occurs as very thin (2–10 µm), partial rims around and within fractures of sodalite (Fig. 12). It also occurs as almost pure end-member $(Ab_{99}An_{0.7}Or_{0.3})$, colourless, prismatic, subhedral crystals up to 300 µm at the boundaries between the fine-grained host rock xenoliths and coarser sodalite–microcline–calcite–dolomite intergrowths.

Ancylite-(Ce)
Ancylite-group minerals are common in carbonatites and carbothermal veins as late-stage minerals associated with Ba–REE carbonates, REE fluorocarbonates, strontianite and baryte. (Knudsen, 1991; Ngwenya, 1994; Wall and Mariano, 1995; Cooper, 1996; Zaitsev et al., 1998; Al Ani and Sarapää, 2013; Dalsin et al., 2015). The mineral is commonly used as an indicator of carbohydrothermal activity, crystallising at temperatures <450°C (Wall and Zaitsev, 2004). Among carbonatite deposits worldwide, ancylite-group mineral compositions indicate significant flexibility in terms of Sr and REE contents, with ancylite-(Ce), Nd-dominant ancylite and ancylite-(La) all being observed (Zaitsev et al., 1998; Reguir and Mitchell, 2000; Petersen et al., 2001).

Ancylite-(Ce) is a late-stage mineral at Mount Mather Creek where it occurs as anhedral-to-subhedral, blocky, translucent-to-opaque, orangepink-to-orangered grains 10 µm to 2 mm in width (av. 150 µm) complexly intergrown with barytocalcite, baryte and edingtonite (Fig. 13). Compositionally, ancylite-(Ce) from Mount Mather Creek shows limited substitution of Ca for Sr (Ca = 0.163–0.230 apfu), with minor Th (av. 0.015 apfu) and Ba (0.010 apfu). It is Ce-dominant (0.447–0.511 apfu), with roughly equal La (0.229–0.348 apfu) and Nd (0.187–0.228 apfu) contents (Table 3). Fluorine contents range from not detectable

Table 7. Representative compositions of fluorapatite from Mount Mather Creek.

Wt. %	Euhedral grain in sodalite syenite									
	Ave. (N = 10)	Min.	Max.	1	2	3	4	5	6	7
SiO_2	0.02	0.01	0.03	0.02	0.03	0.03	0.01	0.03	0.02	0.02
ThO_2	0.05	n.d.	0.17	n.d.	0.09	0.11	n.d.	n.d.	0.03	0.17
UO_2	0.06	0.04	0.08	0.07	0.04	0.08	0.05	0.05	0.05	0.07
Y_2O_3	0.48	0.30	0.77	0.30	0.64	0.77	0.52	0.41	0.58	0.48
La_2O_3	n.d.	n.d.	0.28	n.d.	0.07	n.d.	n.d.	n.d.	0.07	0.28
Ce_2O_3	0.17	0.03	0.44	0.10	0.17	0.40	0.04	n.d.	0.27	0.44
Pr_2O_3	n.d.	n.d.	0.14	n.d.	0.14	0.06	0.09	0.07	n.d.	0.08
Nd_2O_3	0.15	n.d.	0.26	0.12	0.24	0.26	0.10	0.10	0.24	0.20
Sm_2O_3	0.07	n.d.	0.17	n.d.	n.d.	0.11	0.11	n.d.	0.17	n.d.
Eu_2O_3	0.02	n.d.	0.07	n.d.	n.d.	0.05	0.07	n.d.	0.06	n.d.
FeO	0.10	n.d.	0.30	n.d.	n.d.	n.d.	n.d.	n.d.	0.15	0.15
MnO	0.02	n.d.	0.03	0.02	0.02	0.02	0.01	n.d.	0.02	0.01
MgO	n.d.	n.d.	0.03	n.d.	n.d.	n.d.	n.d.	n.d.	n.d.	n.d.
CaO	54.35	53.03	55.07	55.07	54.13	53.03	54.69	54.43	53.92	53.86
SrO	0.23	0.19	0.29	0.20	0.29	0.27	0.26	0.23	0.21	0.27
BaO	0.04	0.00	0.06	0.06	0.03	0.00	0.05	0.04	0.06	0.04
Na_2O	0.27	0.13	0.44	0.15	0.40	0.44	0.23	0.20	0.43	0.38
K_2O	0.01	n.d.	0.03	0.00	0.01	0.03	0.01	n.d.	n.d.	0.01
P_2O_5	42.63	42.11	43.37	42.49	43.27	42.21	43.37	42.52	42.25	42.67
Cl	n.d.	n.d.	0.02	0.02	n.d.	n.d.	0.01	0.01	n.d.	n.d.
F	3.89	3.73	4.32	3.86	3.76	3.73	3.74	3.87	3.93	3.79
$O=F_2,Cl_2$	−1.64	−1.82	−1.57	−1.63	−1.58	−1.57	−1.58	−1.63	−1.65	−1.60
Total	101.02	100.03	101.80	100.89	101.80	100.03	101.79	100.42	100.82	101.33
Formula based on 12 oxygens pfu										
Ca	4.867	4.793	4.955	4.932	4.793	4.797	4.830	4.892	4.859	4.816
Sr	0.011	0.009	0.014	0.010	0.014	0.013	0.012	0.011	0.010	0.013
Ba	0.001	n.d.	0.002	0.002	0.001	n.d.	0.002	0.001	0.002	0.001
Na	0.043	0.021	0.072	0.025	0.064	0.072	0.037	0.032	0.070	0.062
K	0.001	n.d.	0.003	n.d.	0.001	0.003	0.002	n.d.	n.d.	0.001
Fe^{2+}	0.007	n.d.	0.021	n.d.	n.d.	n.d.	n.d.	n.d.	0.011	0.011
Mn	0.001	n.d.	0.002	0.002	0.002	0.001	0.001	n.d.	0.001	0.001
Mg	n.d.	n.d.	0.004	n.d.	n.d.	n.d.	n.d.	n.d.	n.d.	n.d.
Y	0.021	0.013	0.035	0.013	0.028	0.035	0.023	0.018	0.026	0.021
La	0.001	n.d.	0.008	n.d.	0.002	n.d.	n.d.	n.d.	0.002	0.008
Ce	0.005	0.001	0.013	0.003	0.005	0.012	0.001	0.001	0.008	0.013
Pr	0.001	n.d.	0.004	n.d.	0.004	0.002	0.003	0.002	n.d.	0.002
Nd	0.004	n.d.	0.008	0.004	0.007	0.008	0.003	0.003	0.007	0.006
Sm	0.002	n.d.	0.005	0.001	0.001	0.003	0.003	n.d.	0.005	n.d.
Eu	0.001	n.d.	0.002	n.d.	n.d.	0.001	0.002	n.d.	0.002	n.d.
Th	0.001	n.d.	0.003	n.d.	0.002	0.002	n.d.	n.d.	0.001	0.003
U	0.001	0.001	0.001	0.001	0.001	0.001	0.001	0.001	0.001	0.001
Sum	4.971	4.918	5.035	4.992	4.925	4.952	4.918	4.964	5.006	4.961
P	3.016	2.995	3.027	3.007	3.027	3.017	3.027	3.019	3.009	3.015
Si	0.002	0.001	0.003	0.002	0.002	0.003	0.001	0.002	0.002	0.001
Sum	3.018	2.997	3.029	3.008	3.029	3.020	3.028	3.022	3.010	3.016
F	1.028	0.976	1.150	1.021	0.982	0.996	0.976	1.028	1.045	1.000
Cl	0.001	n.d.	0.002	0.002	0.001	n.d.	0.001	0.002	n.d.	n.d.

n.d. – not detected

to 0.244 apfu (av. 0.176 apfu), similar to those observed in ancylite-(Ce) from Khibina carbonatites with 0.148–0.488 apfu F (Zaitsev *et al.*, 1998). The average composition is $(Sr_{0.768}Ca_{0.163}Th_{0.025}Ba_{0.010}Mn_{0.001}Na_{0.001})_{\Sigma 0.969}(Ce_{0.479}La_{0.277}Nd_{0.187}$ $Pr_{0.050}Sm_{0.023}Eu_{0.006}Y_{0.006})_{\Sigma 1.027}(OH_{0.824}F_{0.176})_{\Sigma 1.00}$. All ancylite-(Ce) shows strong enrichment in LREE with Ce>La>Nd and only minor, or below the limit of detection, concentrations of elements heavier than Eu. All REE_N distribution patterns show an overall steep negative slope between La_N and Sm_N. However, two distinct populations exist with respect to Nd and Eu: (1) those with Nd > 0.2 apfu, Eu > 0.007 and Nd/Eu_N < 4, which have a less steep, slightly concave down REE_N pattern between La and Eu; and (2) those with Nd < 0.2 apfu, Eu < 0.005 and Nd/Eu_N > 4, with a straighter negative REE_N profile between La and Eu (Fig. 14). There are no textural differences between these two populations.

Baryte
Baryte is a replacement mineral which forms as thin rims on the edges of barytocalcite crystals, and as very fine-grained (100 μm), blocky-to-prismatic, radiating crystals along cleavage planes in barytocalcite and in cavities (Fig. 15). The dominant substituting elements include Sr (0.013–0.138 apfu) and Ca (0.004–0.050 apfu). Mount Mather Creek baryte has an average composition of $(Ba_{0.963}Sr_{0.066}Ca_{0.021}Na_{0.007}K_{0.001}Ce_{0.001})_{\Sigma 1.060}S_{0.981}O_4$.

Barytocalcite
Barytocalcite occurs in the sodalite syenite segregations as fine-grained (up to 0.6 mm), anhedral-to-subhedral, wedge-shaped to blocky crystals which are always mantled by secondary baryte and sometimes with late-stage Sr-rich calcite (Fig. 15). Barytocalcite is commonly intergrown with ancylite-(Ce) (Fig. 13a). Compositionally, barytocalcite from Mount Mather

Table 7 Continued

| Wt. % | 8 | 9 | 10 | Anhedral grains in host rock | | | | | | |
				1	2	3	4	Ave. (N = 4)	Min.	Max.
SiO_2	0.02	0.02	0.02	0.01	0.01	0.02	0.08	0.03	0.01	0.08
ThO_2	0.03	n.d.	n.d.	0.57	0.01	0.14	n.d.	0.18	n.d.	0.57
UO_2	0.05	0.05	0.06	0.08	0.05	0.05	0.06	0.06	0.05	0.08
Y_2O_3	0.38	0.30	0.38	0.92	0.39	0.44	0.50	0.56	0.39	0.92
La_2O_3	n.d.	n.d.	n.d.	0.25	n.d.	0.15	0.11	0.13	n.d.	0.25
Ce_2O_3	0.17	n.d.	0.07	0.77	0.14	0.39	0.36	0.41	0.14	0.77
Pr_2O_3	n.d.	n.d.	n.d.	0.14	n.d.	n.d.	n.d.	n.d.	n.d.	0.14
Nd_2O_3	0.13	n.d.	0.07	0.46	0.22	0.22	0.29	0.30	0.22	0.46
Sm_2O_3	0.08	0.06	0.07	0.07	0.07	0.06	0.10	0.07	0.06	0.10
Eu_2O_3	n.d.	0.05	n.d.	0.01	0.03	0.05	0.05	0.04	0.01	0.05
FeO	0.26	0.15	0.30	0.09	0.09	0.15	0.09	0.11	0.09	0.15
MnO	0.03	0.00	0.02	0.01	n.d.	0.01	n.d.	0.01	n.d.	0.01
MgO	0.03	n.d.	n.d.	n.d.	n.d.	n.d.	0.01	n.d.	n.d.	0.01
CaO	54.60	54.70	55.05	51.76	54.52	53.23	53.73	53.31	51.76	54.52
SrO	0.20	0.20	0.19	0.31	0.23	0.27	0.17	0.25	0.17	0.31
BaO	0.06	0.06	0.05	0.02	0.05	0.06	0.04	0.04	0.02	0.06
Na_2O	0.18	0.13	0.13	0.89	0.26	0.40	0.33	0.47	0.26	0.89
K_2O	n.d.	0.02	0.01	n.d.	n.d.	n.d.	n.d.	n.d.	n.d.	n.d.
P_2O_5	42.44	42.98	42.11	41.26	42.84	42.15	42.88	42.28	41.26	42.88
Cl	n.d.	n.d.	n.d.	n.d.	n.d.	n.d.	n.d.	n.d.	n.d.	n.d.
F	4.32	3.89	3.98	3.85	4.07	4.16	3.73	3.95	3.73	4.16
$O=F_2,Cl_2$	−1.82	−1.64	−1.67	−1.62	−1.71	−1.75	−1.57	−1.66	−1.75	−1.57
Total	101.18	101.09	100.82	99.91	101.28	100.30	100.96	100.61	99.91	101.28
Formula based on 12 oxygens pfu										
Ca	4.920	4.875	4.955	4.758	4.876	4.837	4.796	4.817	4.758	4.876
Sr	0.010	0.010	0.009	0.016	0.011	0.013	0.008	0.012	0.008	0.016
Ba	0.002	0.002	0.002	0.001	0.002	0.002	0.001	0.001	0.001	0.002
Na	0.030	0.021	0.021	0.149	0.042	0.065	0.053	0.077	0.042	0.149
K	n.d.	0.002	0.001	n.d.	n.d.	n.d.	n.d.	n.d.	n.d.	n.d.
Fe^{2+}	0.018	0.011	0.021	0.007	0.006	0.011	0.006	0.007	0.006	0.011
Mn	0.002	n.d.	0.001	0.001	n.d.	0.001	n.d.	0.001	n.d.	0.001
Mg	0.004	0.001	n.d.	n.d.	n.d.	n.d.	0.001	n.d.	n.d.	0.001
Y	0.017	0.013	0.017	0.042	0.017	0.020	0.022	0.025	0.017	0.042
La	n.d.	0.001	n.d.	0.008	n.d.	0.005	0.003	0.004	n.d.	0.008
Ce	0.005	0.002	0.002	0.024	0.004	0.012	0.011	0.013	0.004	0.024
Pr	n.d.	n.d.	n.d.	0.004	n.d.	n.d.	n.d.	0.001	n.d.	0.004
Nd	0.004	n.d.	0.002	0.014	0.007	0.007	0.009	0.009	0.007	0.014
Sm	0.002	0.002	0.002	0.002	0.002	0.002	0.003	0.002	0.002	0.003
Eu	n.d.	0.001	n.d.	0.000	0.001	0.001	0.002	0.001	n.d.	0.002
Th	0.001	n.d.	n.d.	0.011	n.d.	0.003	n.d.	0.004	n.d.	0.011
U	0.001	0.001	0.001	0.002	0.001	0.001	0.001	0.001	0.001	0.002
Sum	5.016	4.941	5.035	5.039	4.969	4.981	4.917	4.976	4.917	5.039
P	3.021	3.027	2.995	2.996	3.027	3.026	3.025	3.019	2.996	3.027
Si	0.002	0.002	0.002	0.001	0.001	0.002	0.006	0.003	0.001	0.006
Sum	3.023	3.029	2.997	2.997	3.028	3.028	3.031	3.021	2.997	3.031
F	1.150	1.023	1.056	1.044	1.073	1.116	0.984	1.054	0.984	1.116
Cl	n.d.	0.001	n.d.	0.001	n.d.	n.d.	n.d.	n.d.	n.d.	0.001

Creek is almost pure end-member, with an average formula of $(Ba_{1.026}Sr_{0.002})_{\Sigma1.028}(Ca_{0.996}Na_{0.008}Fe^{2+}_{0.001}Ce_{0.001})_{\Sigma1.006}C_{1.983}O_6$ (Table 4). Barytocalcite is not a common carbonatite mineral, having been found only at the Vuoriyarvi, Kovdor and Khibina massifs, Russia (Kapustin, 1980; Zaitsev et al., 1998), Jacupiranga and Araxá, Brazil (Traversa et al., 2001; Costanzo et al., 2006), the Sokli massif, Finland (Vartiainen, 1980), Haast River, New Zealand (Woolley, 2019), Palabora complex, South Africa (Giebel et al., 2017), the Montviel complex, Quebec (Nadeau et al., 2015), Chipman Lake, Ontario (Platt and Woolley, 1990) and the carbonatites at the Ice River complex, British Columbia (Pell, 1994).

Edingtonite and a potentially-new Mg-bearing edingtonite-like mineral

Edingtonite, $BaAl_2Si_3O_{10}\cdot4H_2O$, is a rare Ba-zeolite which has only been found at four other localities in Canada: (1) Zinc Mountain ridge in the Ice River alkaline complex, 25 km south of Field, British Columbia (Grice et al., 1984); (2) at the Brunswick No. 12 Pb–Cu–Zn mine, 2350 level, East Stope, near Bathurst, New Brunswick (Grice et al., 1984); (3) from a single miarolitic cavity in nepheline syenite at Mont Saint-Hilaire, Quebec (Horváth et al., 2019); (4) from the Gun claim, a Ba-rich skarn deposit, Yukon (Dunning et al., 2018). At the Ice River alkaline complex, edingtonite occurs as euhedral white crystals ($8 \times 2 \times 2$ mm) in late-stage zeolite plus carbonate-rich pockets in nepheline syenite, associated with calcite and natrolite, together with rare ancylite, catapleiite, aegirine, pyrite and galena (Grice et al., 1984). It has also been found in carbonatites in the Khibina massif, Kola Peninsula (Zaitsev et al., 1998).

At Mount Mather Creek, initial examination, semi-quantitative energy-dispersive spectroscopy and PXRD indicated the presence of edingtonite as a late-stage mineral in fractures and pockets of

Table 8. Representative compositions of quintinite from Mount Mather Creek.

Wt.%	1	2	3
SiO_2	0.07	0.08	0.04
Al_2O_3	19.96	20.38	20.38
FeO	9.31	8.90	9.33
MgO	26.07	26.75	26.07
H_2O (calc)	31.59	32.12	31.81
CO_2 (calc)	8.58	8.72	8.63
Total	95.58	96.95	96.26
Formulae calculated on the basis of 6 cations pfu, 3 H_2O pfu and 1 CO_3 pfu			
Si	0.006	0.007	0.003
Al	2.009	2.018	2.038
Fe^{2+}	0.665	0.625	0.662
Mg	3.320	3.350	3.297
H_2O	3.000	3.000	3.000
CO_3^{2-}	1.000	1.000	1.000
OH^-	12.000	12.000	12.000
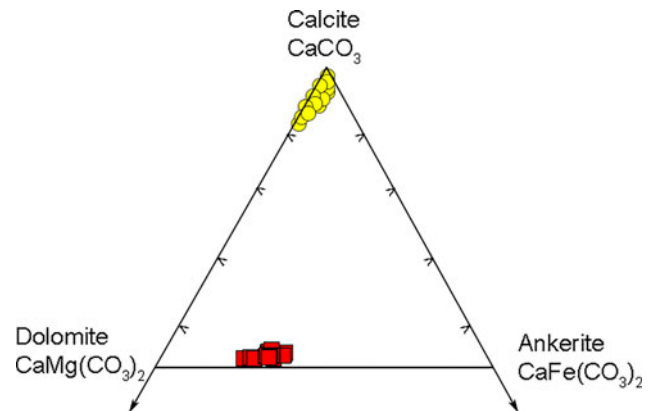
Fig. 6. Ca–Mg–Fe ternary diagram representing the composition of the main carbonates at Mount Mather Creek. Calcite = yellow circles; ferroan dolomite = red squares.

the sodalite syenite (Fig. 16a). It occurs as anhedral, transparent, colourless-to-beige crystals associated with ancylite-(Ce), barytocalcite, calcite and sodalite. The average composition of Mount Mather Creek edingtonite, based on 14 oxygens pfu, is $(Ba_{0.846}Ca_{0.130}K_{0.085}Na_{0.059}Sr_{0.012}Mg_{0.012}Ti_{0.003}Fe^{2+}_{0.002}Mn_{0.001}Zn_{0.001})_{\Sigma1.152}Al_2(Si_{2.788}Al_{0.219})_{\Sigma3.007}(O_{9.973}F_{0.024}Cl_{0.002}S_{0.001})_{\Sigma10.000}\cdot4H_2O$ (Table 5). This composition is similar to that given by Grice *et al.* (1984) and Gatta and Boff Ballaran (2004) for edingtonite from the Ice River complex, $(Ba_{0.98}K_{0.03}Na_{0.01})_{\Sigma1.02}(Al_{1.96}Si_{0.02})_{\Sigma2.00}Si_{3.16}O_{10}\cdot3.68H_2O$. High analytical totals are the result of either beam damage or dehydration of the mineral prior to analysis. Edingtonite from Mount Mather Creek is the tetragonal polymorph, $P\bar{4}2_1m$, $a = 9.5968(2)$, $b = 6.5365(3)$ Å and $V = 602.01(4)$ Å^3.

Closer examination has revealed the presence of not only edingtonite, *sensu stricto*, but also of an unknown Mg-bearing edingtonite-like mineral. The PXRD pattern of the unknown revealed extra peaks not present in the ideal edingtonite pattern (Table 6). Furthermore, when the formula is calculated based on 14 oxygens pfu, EPMA show consistent excess Mg (∼0.25 apfu) not required to fill any of the three cation sites. Detailed PXRD and unit cell refinement indicate that the unknown mineral

is orthorhombic, point group 222, with $a = 13.8556(3)$, $b = 13.6794(19)$ and $c = 13.7236(4)$ Å and $V = 1251.11(7)$ Å^3. The average formula based on 56 oxygens pfu is $(Ba_{3.453}Sr_{0.274}K_{0.106}Na_{0.100}Ca_{0.072})_{\Sigma4.084}(Mg_{0.920}Fe^{2+}_{0.020}Ti_{0.008}Zn_{0.004}Mn_{0.005})_{\Sigma0.957}(Al_{9.597}Si_{0.308})_{\Sigma9.905}Si_{10}(O_{39.933}F_{0.060}Cl_{0.004}S_{0.003})_{\Sigma40.000}\cdot16H_2O$ (Table 5), and a general formula of $Ba_4MgAl_{10}Si_{10}O_4\cdot16H_2O$. Compositionally it is related to edingtonite by the coupled substitution $2Si^{4+} + \square \leftrightarrow Mg^{2+} + 2Al^{3+}$ (where $\square$ = vacancy).

As with edingtonite, the potentially-new Ba–Mg silicate is found intergrown with ancylite-(Ce) and barytocalcite (Fig. 16b). Crystals are colourless to light beige, vitreous to slightly waxy, anhedral, with an average size of 60×40 µm. Back-scattered electron images indicate compositional zoning with Mg ↔ Ca (Fig. 16b).

Other zeolite minerals include analcime, gonnardite, harmotome, chabazite-Na and natrolite. Analcime occurs as a secondary mineral along fractures in sodalite and in vugs. Chabazite-Na occurs as very fine grained (5–20 µm), pseudocubic crystals with rare penetration twins in vugs along with quintinite and secondary calcite (Fig. 10). Natrolite occurs in radiating sprays of colourless, prismatic crystals up to 3 mm long associated with microcline and sodalite.
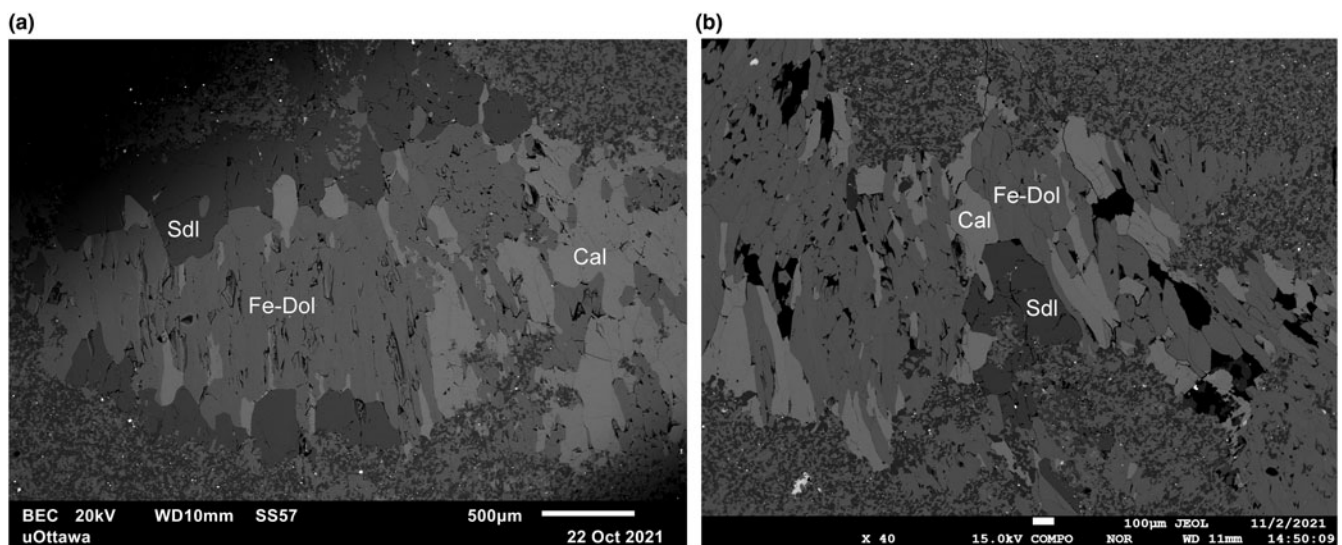
Fig. 5. Back-scattered electron image of a comb-textured vein comprised of (a) calcite (Cal) and (b) ferroan dolomite (Fe-Dol) bordered by sodalite (Sdl).
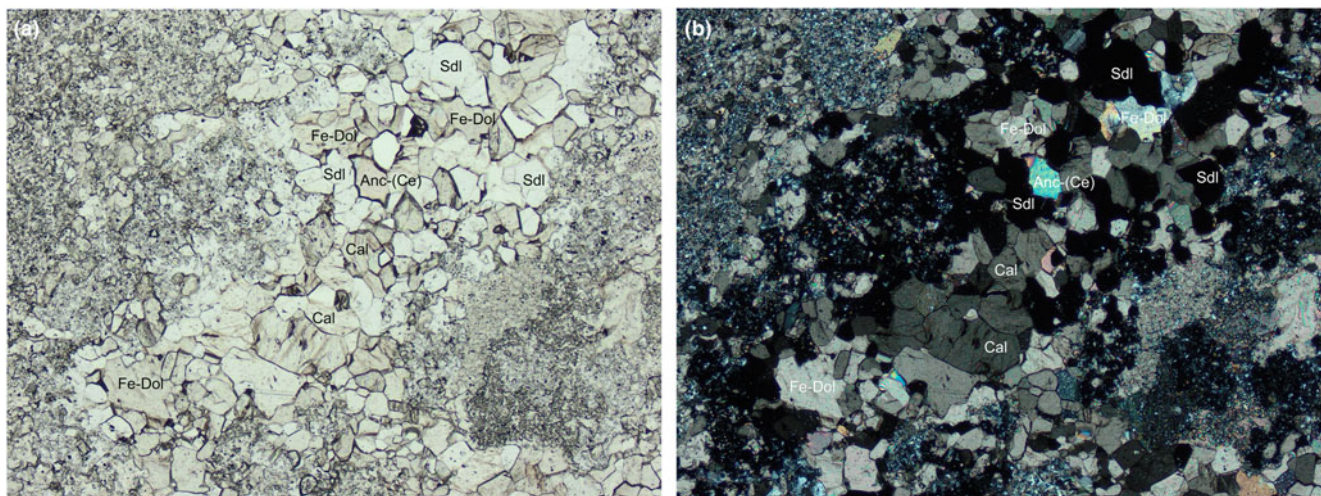
Fig. 7. Bands of fine-grained sodalite, calcite and ferroan dolomite at Mount Mather Creek in plane polarised light (a) and cross-polarised light (b). Field of view = 4 mm.

Fluorapatite

Apatite occurs in both the breccia groundmass and in carbonate veins. In the breccia, it occurs as rare euhedral, prismatic crystals up to 0.75 mm in length associated with sodalite, microcline and calcite (Fig. 17). Within the carbonate veins, apatite occurs as fine-grained (60–100 μm), anhedral, commonly rounded, elongated grains in a granular texture with calcite and dolomite. All apatite is Cl-poor, F-dominant fluorapatite with Sr = 0.009–0.016 apfu (0.19–0.31 wt.% SrO) Mn = b.d.l.–0.002 apfu (b.d.l–0.03 wt.% MnO), Na = 0.021–0.149 apfu (0.13–0.89 wt.% Na$_2$O; Table 7). Back-scattered electron images reveal the euhedral groundmass crystals to have oscillatory zoning, with brighter core zones enriched in Sr and ΣREE relative to the rims and base of the crystals (darker zones, Fig. 17a). Zoning was also observed in CL images, with luminescence ranging from light yellow at the rims to green and orange–pink in the cores (Fig. 17b). No compositional zoning was observed in the fine-grained fluorapatite in the host rock. Using the SrO *versus* MnO wt.% diagram developed by Hogarth (1989), Mount Mather Creek fluorapatites

from the sodalite syenite plot within the overlapping skarn, phosphorite and carbonatite fields whereas those from the host rock plot within the skarn–carbonatite field. (Fig. 18).

Quintinite

Quintinite, Mg$_4$Al$_2$(OH)$_{12}$CO$_3$·3H$_2$O, is a rare Mg–Al–CO$_3$ layered double hydroxide, a member of the quintinite group and the hydrotalcite supergroup. It is a late-stage hydrothermal mineral found dominantly in alkaline rocks including carbonatites, pegmatites and miariolitic cavities in nepheline syenite, and phoscorites (Chao and Gault, 1997; Zhitova *et al.*, 2018), serpentine–magnesite deposits (Raade, 2013), altered gabbros (Zhitova *et al.*, 2017), basaltic volcaniclastic sediments and iron mines (e.g. Långban, Sweden; (Strand, 2016). Quintinite-group minerals are defined by having a M^{2+}:M^{3+} ratio of 2:1 with CO$_3^{2-}$ or Cl$^-$ and H$_2$O in the interlayer; the general formula for the group is given as $M_4^{2+}M_2^{3+}$(OH)$_{12}$(CO$_3$)·3H$_2$O (Mills *et al.*, 2012; Zhitova *et al.*, 2018). A diverse array of quintinite polytypes
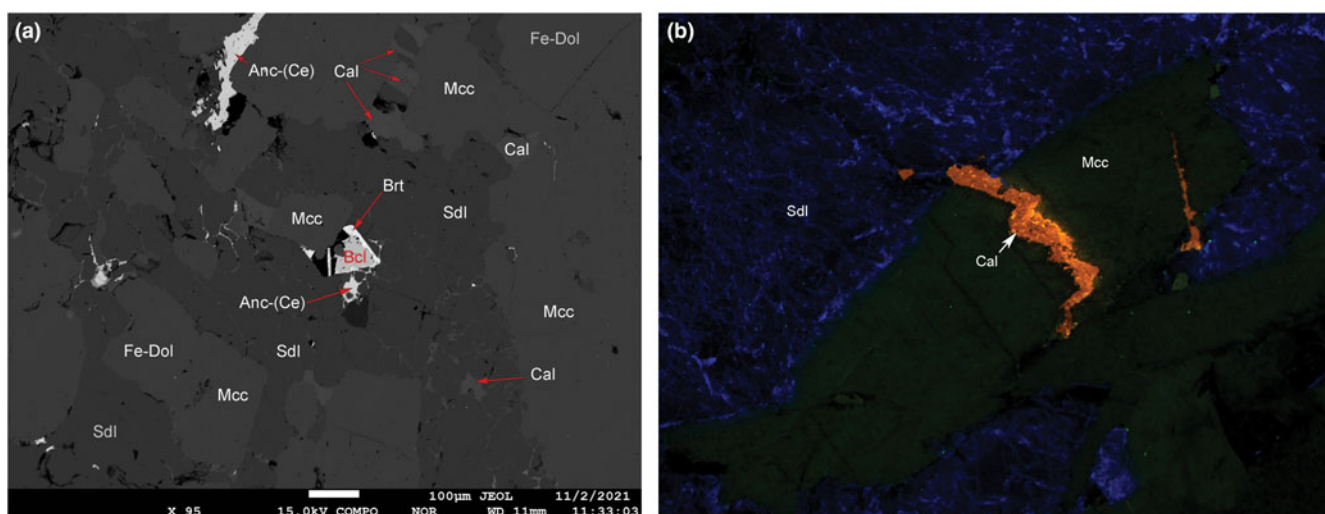
Fig. 8. (a) Back-scattered electron image showing calcite replacing sodalite along fractures. (b) Cathodoluminescence image showing calcite overgrowing microcline. Field of view = 3 mm, abreviations as in Fig. 4.
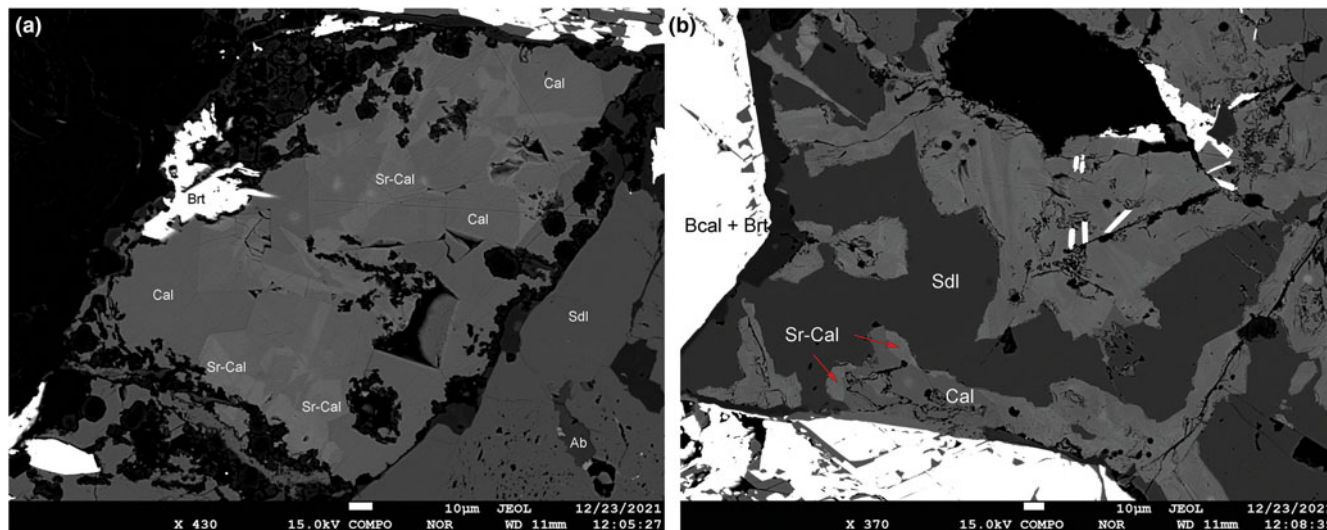
Fig. 9. Back-scattered electron image depicting complex replacement textures and intergrowths of calcite and Sr-rich calcite after sodalite. Abreviations as in Fig. 4.

have been observed, although intergrowths of two or more polytypes are common.

Mount Mather Creek is only the second occurrence of quintinite in Canada, together with the type locality Mont Saint-Hilaire, Quebec (Chao and Gault, 1997). It is found in small vugs within the sodalite syenite matrix, commonly coated with cubes of chabazite-Na or secondary calcite, together with ancylite-(Ce), microcline and sodalite (Fig. 10). Quintinite occurs as translucent, light yellow, euhedral (pseudo)hexagonal prisms up to 150×100 µm (average: 70×40 µm; Fig. 19a). Many of the crystals are capped with an epitactic overgrowth of quintinite of the same composition (Fig. 19b–d). Further structural studies are being completed to determine the polytypes and determine the mechanism and conditions responsible for the epitaxial overgrowths. Initial PXRD data coupled with Rietveld analyses indicate the crystals to be a mixture quintinite-1*M* and quintinite-3*T*, however unresolved peaks remain in the residua of the patterns.

The average composition of quintinite from Mount Mather Creek is $(Mg_{3.322}Fe^{2+}_{0.651})_{\Sigma3.973}(Al_{2.022}Si_{0.005})_{\Sigma2.027}(OH)_{12}(CO_3)$
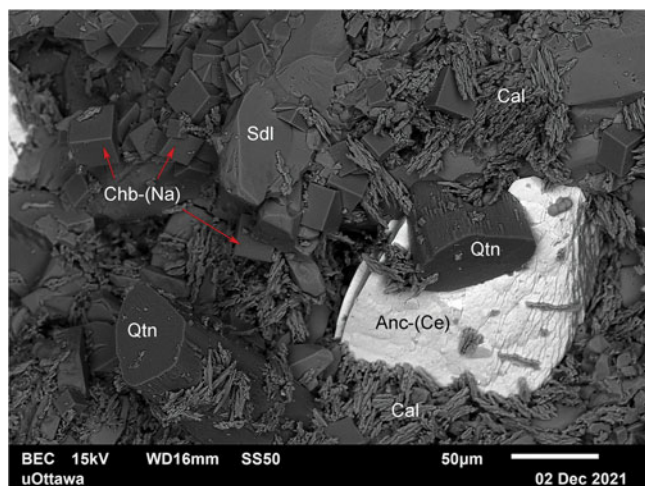
Fig. 10. Back-scattered electron image of drusy calcite in a vug with ancylite-(Ce), chabazite-Na, quintinite and sodalite. Abreviations as in Fig. 4.

$\cdot 3H_2O$. The analytical totals in Table 8 range from 95.58 to 96.95 wt.%, a function of the high volatile nature of the samples ($\sim$45 wt.%) and the pronounced basal parting leading to volatile migration. Notably Mount Mather Creek quintinite is enriched in Fe^{2+} (0.651 apfu) relative to the type material from Mont Saint-Hilaire (0.05 apfu Fe_{tot}) and the Jacupiranga mine, Brazil (0.12 apfu Fe_{tot}); only one sample of quintinite-3*R* from the Kovdor phoscorite–carbonatite complex, Kola peninsula, Russia, has a higher Fe content (1.02 apfu; (Zhitova *et al.*, 2018). Chao and Gault (1997) suggested an extensive solid solution series between quintinite and caresite, the Fe-end member, and noted that an intermediate member with Mg:Fe = 2.01:2.00 apfu has been found at Mont Saint-Hilaire, however no analyses were published. There is no evidence for a solid-solution series between quintinite and the Mn end-member, charmarite; Mn was not detected in quintinite from Mount Mather Creek, Mont Saint-Hilaire, or the Kovdor massif. Precipitation synthesis at 85°C and thermal decomposition experiments up to 1000°C of charmarite indicate that the interlayer H_2O is less stable than that in quintinite (Grand *et al.*, 2010). In addition, at these conditions, increased Mn activity, the formation of Mn_3O_4, bayerite and rhodochrosite is more favourable than charmarite (Grand *et al.*, 2010). It may be that in the low-temperature hydrothermal environments that quintinite is formed, the increased ionic radius of Mn^{2+} *versus* Mg^{2+} results in a compositional miscibility gap and a solid solution between quintinite and charmarite is not possible.

Nordstrandite

Nordstrandite is one of four naturally-occurring $Al(OH)_3$ polymorphs together with gibbsite, bayerite and doyleite. It is generally considered to be a low-temperature alteration product, found in bauxite deposits associated with carbonate or alkaline rocks, in dolomitic oil shales, as an alteration product of dawsonite and alumohydrocalcite, and a late-stage mineral in pegmatites and miarolitic cavities in nepheline and sodalite syenites (Chao and Baker, 1982; Kovács-Pálffy *et al.*, 2008). Of all the $Al(OH)_3$ polymorphs, nordstrandite is the rarest in nature, however it is the most common polymorph found in SiO_2-undersaturated alkaline intrusions worldwide including at Mont Saint-Hilaire and the Saint-Amable sill, Quebec (Chao and Baker, 1982;
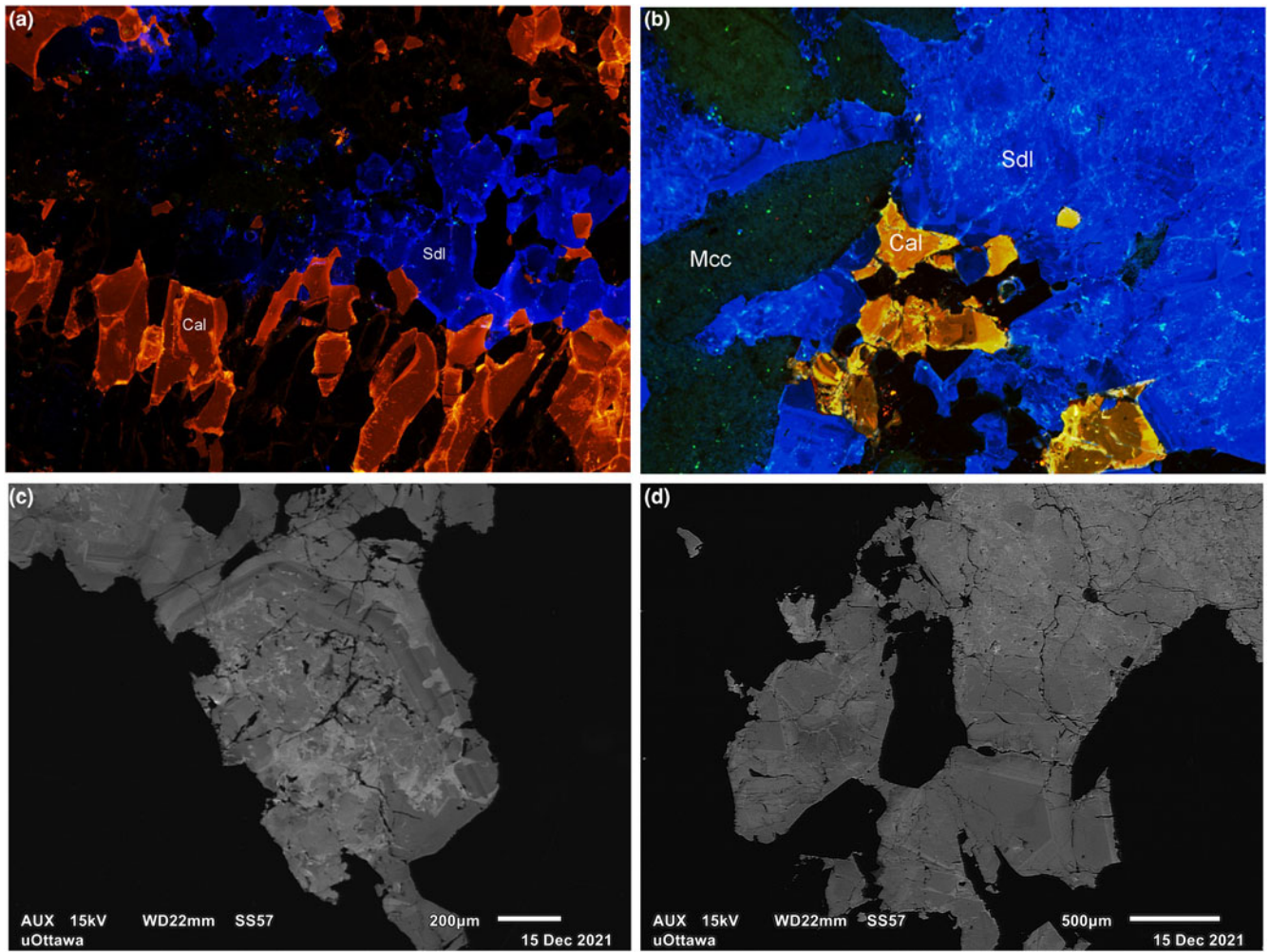
Fig. 11. (a,b). Bright blue luminescence of sodalite. Field of view = 3 mm. (c,d) Monochromatic CL image of sodalite showing primary oscillatory zoning and patchy, mottled textures. Abreviations as in Fig. 4.

Horváth, 2010), the Princess Sodalite Mine, Bancroft, Ontario, Canada (Sabina, 1982), the Cerro Sapo deposit, Ayopaya province, Brazil (L. Hováth, pers. comm.), Narssârssuk, Greenland (Petersen *et al.*, 1976), the Larvik Plutonic Complex, Norway (Larsen, 2010), and the Khibina, Kovdor and Lovozero massifs, Russia (Zaitsev, 1996; Pekov, 2000; Yakovenchuk *et al.*, 2005)
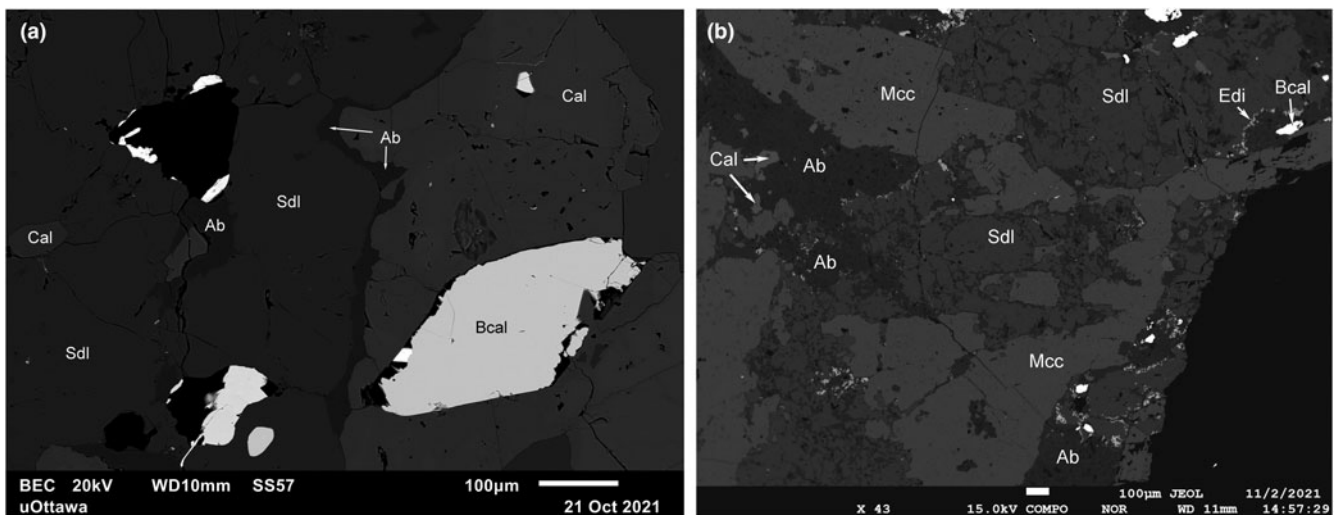
Fig. 12. Back-scattered electron images of sodalite altering to albite. Abreviations as in Fig. 4.
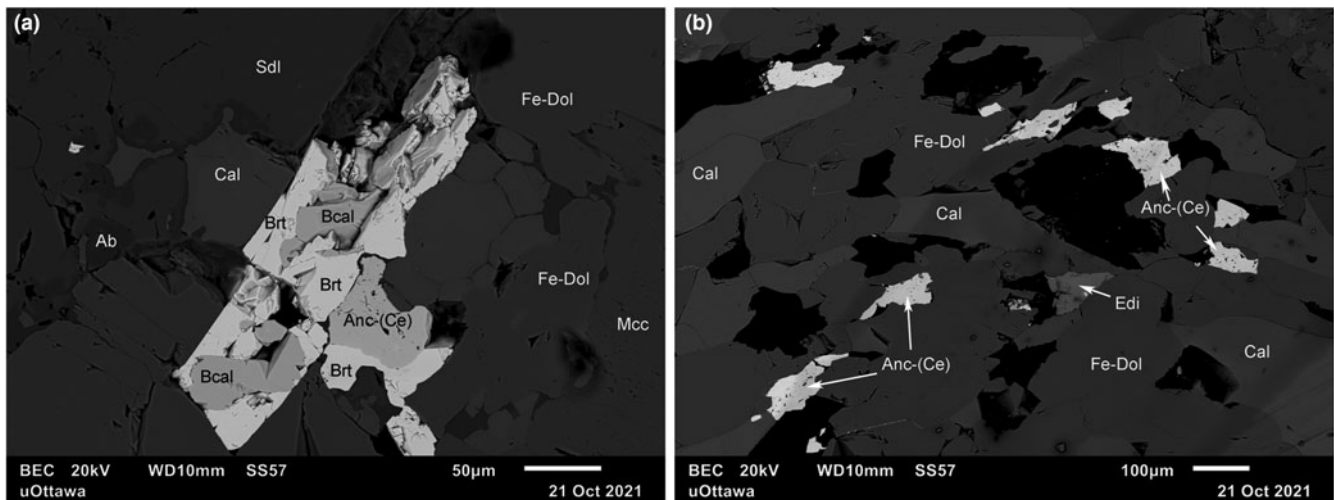
Fig. 13. Back-scattered electron images of ancylite-(Ce) associated with barytocalcite, baryte and edingtonite. Abreviations as in Fig. 4.

where it occurs in pegmatites, veins and miarolitic cavities, and is typically the last mineral to form in the paragenetic sequence. Unfortunately, little is known about the stability and conditions of formation of nordstrandite in these alkaline environments. Studies of the alumina–water system have been limited to ambient pressures and temperatures in aqueous systems which mimic conditions in soils (Barnhisel and Rich, 1965; Violante and Huang, 1993).

Nordstrandite at Mount Mather Creek occurs as a late-stage mineral, an alteration product after sodalite and possibly albite. It occurs as anhedral, interstitial blebs up to 0.5 mm wide, frequently concentrated along fractures and in regions with other late-stage minerals including edingtonite, baryte and barytocalcite (Fig. 15b). Compositionally, it is almost pure $Al(OH)_3$ with minor Mg (up to 0.93 wt.% MgO) and Si (up to 1.94 wt.% SiO_2).

Sulfides
Galena, pyrite and sphalerite occur in trace amounts within both the syenite/carbonatite and within the host rock. Galena occurs as euhedral cubes or anhedral masses dominantly within the host rock clasts. Pyrite occurs as very fine- to fine-grained (10–25 μm) euhedral grains disseminated throughout the host rock and concentrated in fine veinlets with calcite. It is more rarely found as coarser grained, 2 mm cubes associated with galena. Sphalerite occurs as honey yellow to yellow–green metallic, anhedral crystals averaging 1 mm in size within the sodalite syenite matrix. It also occurs mantling galena with pyrite.

Discussion

Within the Foreland Belt of the British Columbia Alkaline Province, REE-bearing carbonatite dykes, sudations and breccias have been noted at a number of localities including the Aley carbonatite, the Wicheeda Lake alkaline complex, the Ice River alkaline complex and the Kechika River area (Pell, 1994). In all cases, these late-stage carbonatites or carbohydrothermal rocks are associated with SiO_2-understaturated syenites, are generally small (0.5–2 m wide), cross-cut the earlier alkaline rocks and are most common in the outer alteration halo (Currie, 1976; Pell, 1994). Geochemically, they are ferroan dolomite, or siderite carbonatites enriched in REE, Ba, Sr and F, in contrast to the main dolomite

carbonatites of the complexes which tend to be enriched in Nb, Zr and Th. Mineralogically, late-stage dykes are notably different than main complex carbonatites as they do not contain common phases such as REE-fluorocarbonates, fluorite, magnetite, monazite, ilmenite, phlogopite, perovskite, pyrochlore and Nb–Ta-oxides, but are instead dominated by carbonate minerals including Ba and REE carbonates, in addition to zeolites (analcime, edingtonite and natrolite) and feldspathoids (sodalite). The Rock Canyon Creek deposit is the only one in the British Columbia Alkaline Province which is not associated spatially with outcrops of carbonatite or other alkaline rocks.

As with the Rock Canyon Creek deposit, there is no field evidence to support the presence of a parental syenite or carbonatite for the Mount Mather Creek breccia. The nearest occurrence is the Ice River Complex, located ~64 km to the southeast. The brecciated, stockwork nature of the Mount Mather Creek deposit suggests proximity to a parental body, though it is extremely unlikely that Ice River is the source of the silicate–carbonate fluids given the geographical distance. The parental body remains a mystery, however an unexposed intrusion remains a possibility. Although no consanguineous alkaline intrusion has been observed, most sodalite-bearing rocks are associated with nepheline-bearing intrusions. In order to generate the highly fractionated fluids from which the veins at Mount Mather Creek and other localities are derived, an earlier-crystallising intrusion must be present from which the fluids/melts evolved.

The paragenetic sequences for the Mount Mather Creek breccia are given in Fig. 4. On the basis of textural relationships and mineral composition, three dominant paragenetic stages of formation are proposed: (1) intrusion and brecciation of the host rock by a Cl-rich carbonated silica-bearing fluid/melt; (2) late-stage formation of REE+Na+Ba+Sr minerals; and (3) alteration of primary silicate and carbonate phases by CO_2–H_2O fluids and late-stage, post-magmatic crystallisation. In summary:

$$\text{sodalite} + \text{microcline} + \text{ferroan dolomite} + \text{calcite} + \text{fluid} \quad (1)$$

$$\text{albite} + \text{zeolites} + \text{nordstrandite} + \text{quintinite}$$
$$+ \text{ancylite-(Ce)} + \text{barytocalcite} \quad (2)$$

$$\text{baryte} + \text{Sr-calcite} + \text{chabazite-Na} + \text{calcite} \quad (3)$$
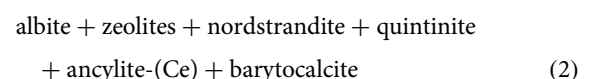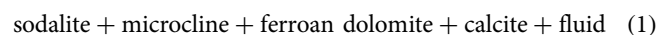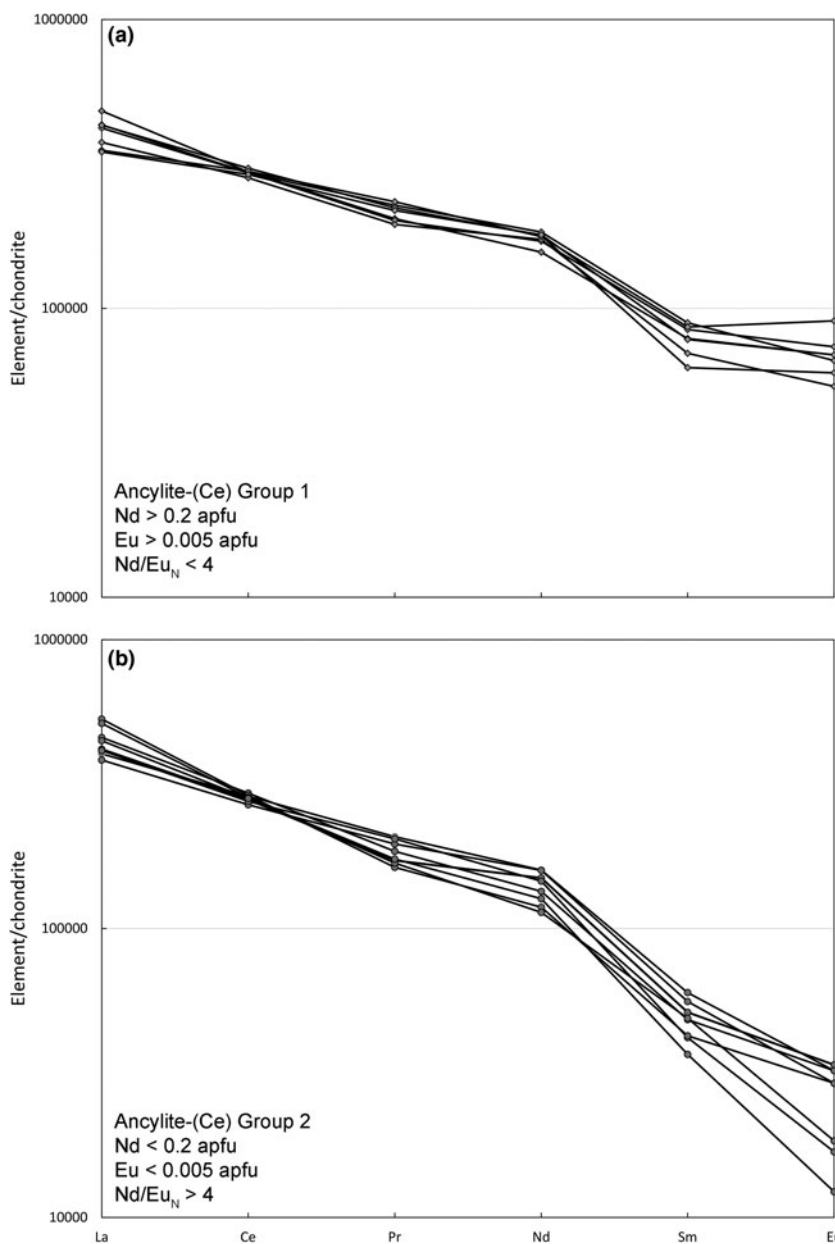
Fig. 14. Chondrite-normalised rare earth element patterns for the two populations of ancylite-(Ce): those with those with (a) Nd > 0.2 apfu, Eu > 0.005 apfu and Nd/EuN < 4, and (b) Nd < 0.2 apfu, Eu < 0.005 apfu and Nd/EuN > 4.

The dominant breccia matrix assemblage of ferroan dolomite, calcite, sodalite and microcline suggests that the original melt was of mixed silicate-carbonate composition and not a *bona fide* carbonatite associated with alkaline rock – carbonatite complexes such as the type locality Fen complex, Norway (Mitchell, 2005). The presence of primary sodalite in the dyke rather than nepheline can be attributed to two possible process, both of which require a NaCl-enriched melt: (1) early crystallisation of nepheline resulting in an increase in the NaCl content of the melt and later crystallisation of sodalite which, being less dense than nepheline, would become buoyant in the upper magma chamber; or (2) the primary melt was sufficiently enriched in NaCl to crystallise sodalite first, leaving behind a parental melt depleted in NaCl from which nepheline would later crystallise (Sharp *et al.*, 1989). In both scenarios, primary sodalite is observed in the dyke whereas the parental body would be composed dominantly of nepheline syenite. The presence of sodalite syenite within the upper layers of larger alkaline intrusions has

been observed at Mont Saint-Hilaire (Horváth *et al.*, 2019), Ilímaussaq, South Greenland (Sørensen, 1958) and the Lovozero massif, Russia (Vlasov *et al.*, 1966; Pekov, 2000), where sodalite buoyancy and crystal flotation has been used to explain the stratification and downward enrichment of silica (Sharp *et al.*, 1989). The same mechanism can be invoked for the presence of sodalite syenite in volatile-rich dykes at Mount Mather Creek and other localities because less dense, buoyant sodalite is easily removed from the magma chamber and transported in the melt *via* fractures into the surrounding host rock.

The REE–Na–Ba–Sr–Cl-rich mineral assemblage found within the breccia, in particular ancylite-(Ce), is indicative of hydrothermal or carbohydrothermal rather than primary magmatic processes (Zaitsev *et al.*, 2014). Flow textures within the alternate bands of the breccia, as well as textures between the minerals themselves, indicate concomitant crystallisation of carbonate and silicate minerals from a single parental melt/fluid. Host rock clasts entrained in the matrix might have contributed
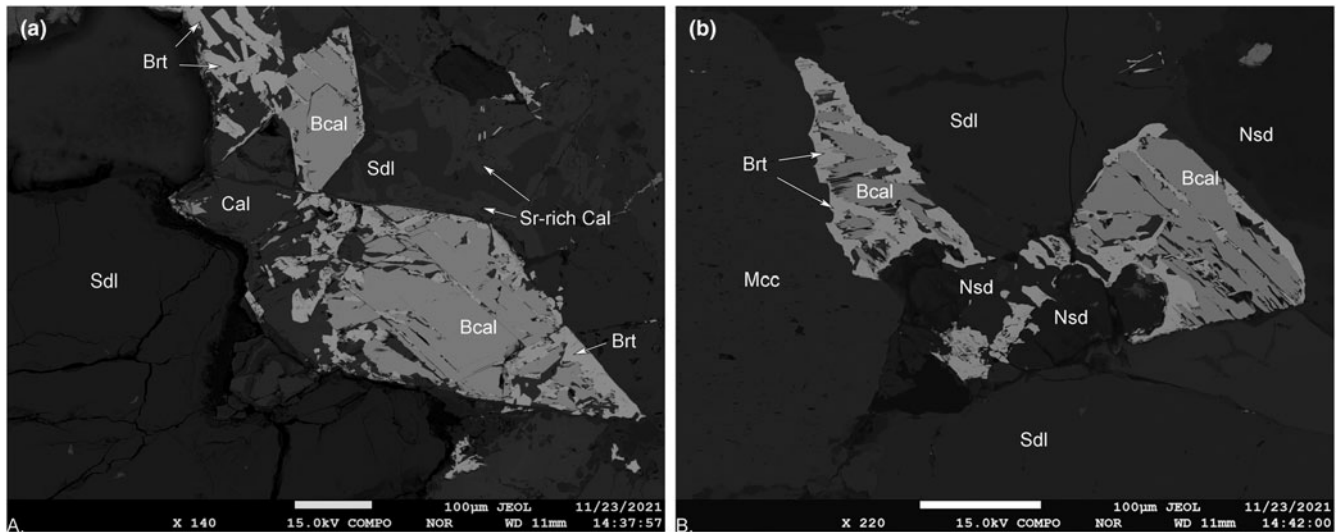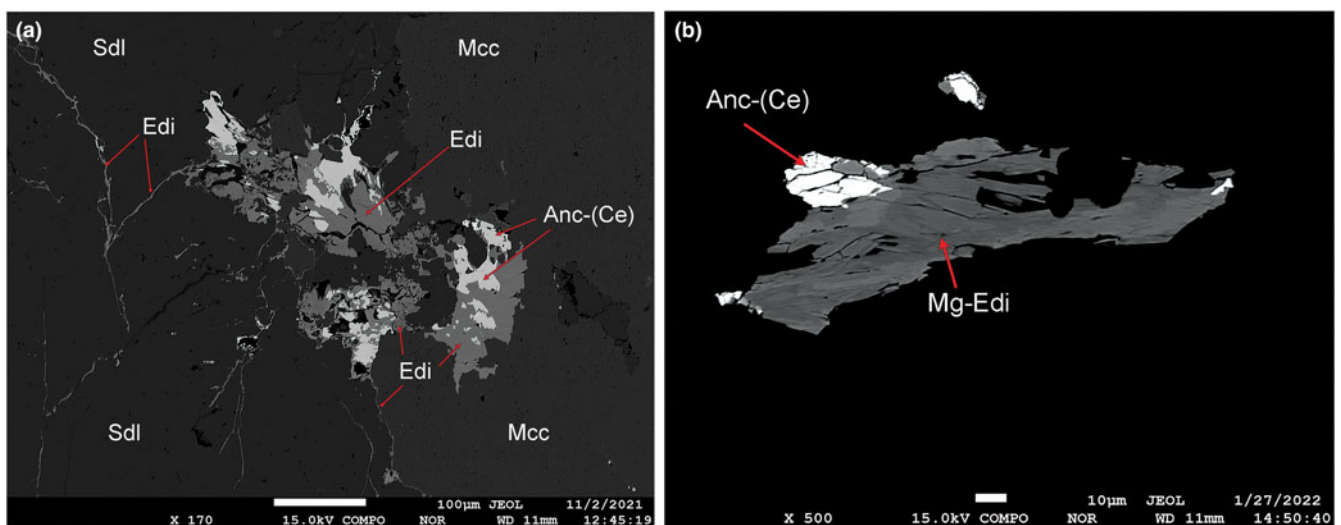
Fig. 15. Back-scattered electron images of barytocalcite with sodalite, calcite and ferroan dolomite being replaced by baryte, calcite, Sr-rich calcite (a) and nordstrandite (b). Abreviations as in Fig. 4.

chemically to the dyke, however the bulk composition of the host rock (albite, calcite and dolomite) would have been very similar to that of the intruding melt. Determining the degree to which wall-rock interactions played a role in the resultant mineralogy would require isotopic analyses.

Mount Mather Creek shows many similarities to a sodalite–ankerite–baryte dyke observed in the Cerro Sepo area of the Ayopaya alkaline province, Bolivia (Schultz *et al.*, 2004) which consists of rhythmically-layered ankerite and baryte with bands or irregular patches of monomineralic dark blue sodalite with crystals reaching up to 9 cm. The textures in the dyke indicate concomitant crystallisation of carbonates and sodalite (Schultz *et al.*, 2004). The dyke cross-cuts nepheline syenite, the contact between which is strongly brecciated with an intense sodalite–ankerite stockwork and narrow zones of fenitisation, very similar to that observed at Mount Mather Creek (Schultz *et al.*, 2004). The Cerro Sepo dyke also contains a diverse suite of minor

minerals including calcite, microcline, natrolite, analcime, sulfides (galena, sphalerite, pyrite and chalcopyrite) as well as REE–Sr–Th-rich minerals including strontianite, Sr-apatite, goyazite, mckelveyite and bellbergite. Unlike at Mount Mather Creek, at Cerro Sepo, the dyke has a well-defined genetic relationship with the nepheline syenite, which contains late-stage magmatic sodalite with carbonate inclusions, indicating carbonate saturation in the residual magma (Schultz *et al.*, 2004). The unique sodalite–ankerite–baryte dyke is interpreted to represent a highly-fractionated, peralkaline, carbonated silicate melt enriched in Na, Cl, Ba, Sr, F, Th and REE, or, in other words, a carbohydrothermal residuum (Zaitsev, 1996; Mitchell, 2005).

At Mount Mather Creek, the primary silicate + carbonate assemblage has undergone alteration, resulting in a secondary assemblage of REE–Ba–Sr–Na phases including albite, analcime, cancrinite, gonnardite and nordstrandite after sodalite, as well as complex intergrowths of ancylite-(Ce), barytocalcite, edingtonite

Fig. 16. (a) Back-scattered electron image of edingtonite (Edi) with ancylite-(Ce) [Anc-(Ce)], as stringers in sodalite (Sdl), and at the contacts with microcline (Mcc).
(b) Back-scattered electron image of the potentially-new Mg-bearing edingtonite-like mineral (Mg-Edi) with ancylite-(Ce) [Anc-(Ce)].
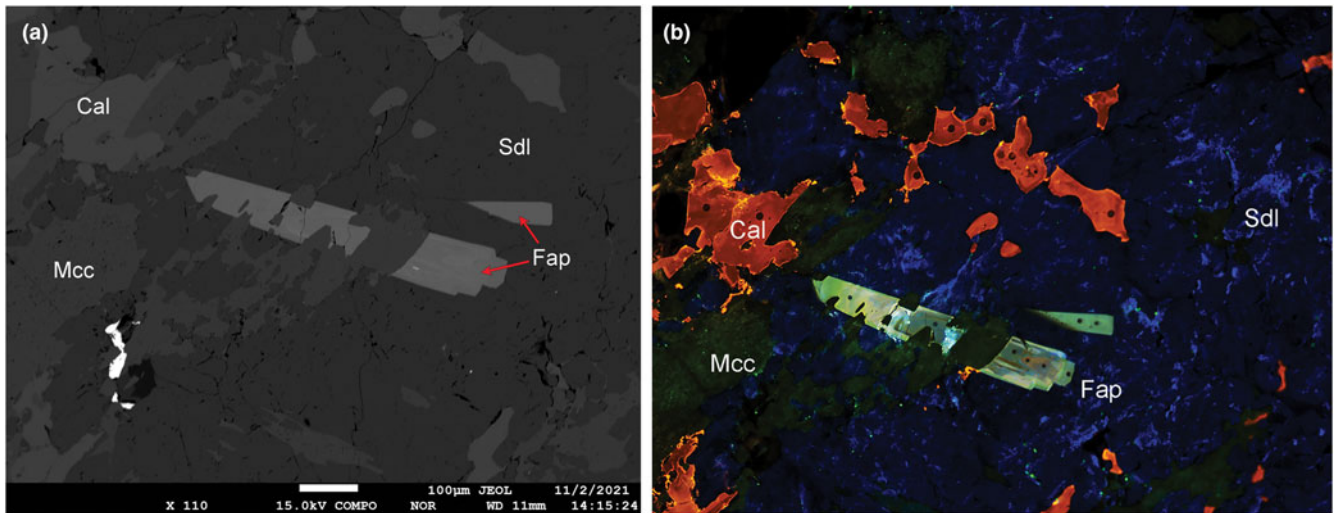
Fig. 17. (a) Back-scattered electron image of fluorapatite showing compositional zoning. (b) Cathodoluminescence image showing compositional zoning in the fluorapatite with luminescence ranging from yellow to green to orange-pink. Field of view = 3 mm, abreviations as in Fig. 4.

and a potentially new Mg-bearing edingtonite-like mineral. The presence of the $Al(OH)_3$ polymorph nordstrandite in the late stages of crystallisation supports a SiO_2-undersaturated alkaline melt and indicates remobilisation of Al from earlier phases (i.e. sodalite). Although there still exists much debate on the exact conditions of formation of the $Al(OH)_3$ polymorphs, and relationships in the Al–O–H system in general, under geological conditions, it is generally agreed that nordstrandite is the high pH polymorph (7.5–9), is unstable at high SiO_4^{4-} activities and requires an intermediate rate of dissolution and nucleation of Al–OH polymers (Violante and Huang, 1993; Kawano and Tomita, 1996; Ramesh, 2012). There is also evidence to suggest that nucleation of Al–OH polymers and growth of nordstrandite is enhanced in the

presence of Cl^- (Peskleway et al., 2005), in this case as a result of breakdown of sodalite, and would thus be more stable in melts enriched in NaCl rather than more acidic F-bearing melts.

The fluids responsible for these secondary assemblages had to have been enriched in Na_2O, CO_2 and H_2O, as well as Ba, Sr and LREE. Recently, REE have been shown to be highly soluble and easily transported long distances in alkali (Na)-rich carbonatitic fluids, with anionic species (Cl^-, F^- or CO_3^{2-}) being less important factors (Anenburg et al., 2020). In contrast, in alkali-free carbonatitic melts, REE have low mobility and are hosted in insoluble REE carbonates and phosphates within the carbonatite body itself, rather than in external dykes. Similarly, assimilation of siliceous material by carbonatite melt results in incorporation of REEs
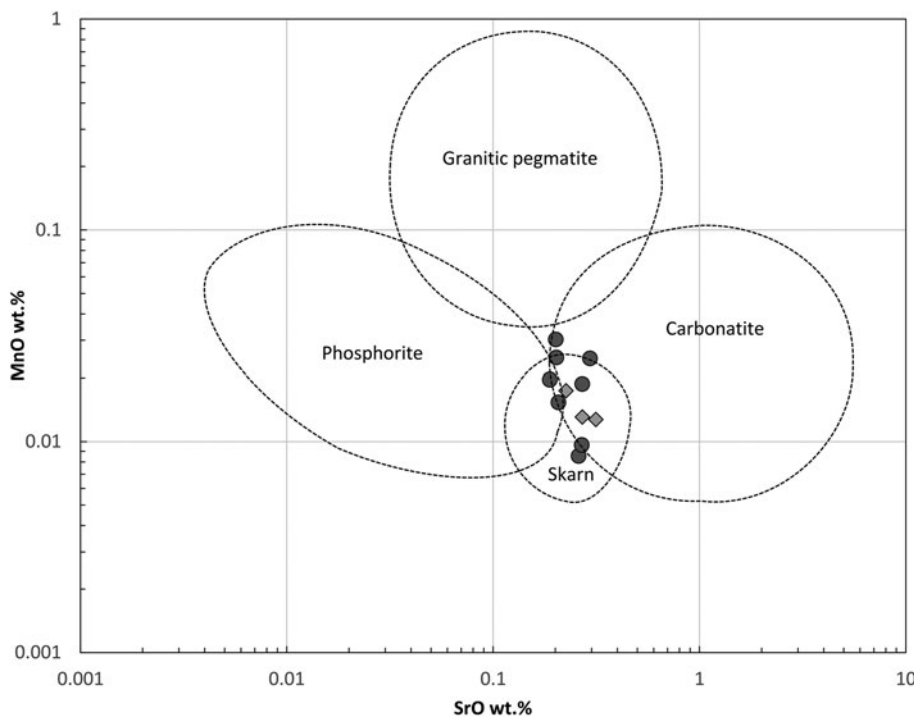
Fig. 18. Compositional variation of Mn and Sr (wt.%) in Mount Mather Creek fluorapatite compared with apatites from phosphorites, granitic pegmatites, skarns and carbonatites; data compiled by Hogarth (1989). Analyses from the large, euhedral fluorapatite from the sodalite syenite (circles) plot at the intersection of the skarn, phosphorite and carbonatite fields, whereas the anhedral fluorapatite from the host rock (grey diamonds) plot within the skarn and carbonatite fields with two outliers.
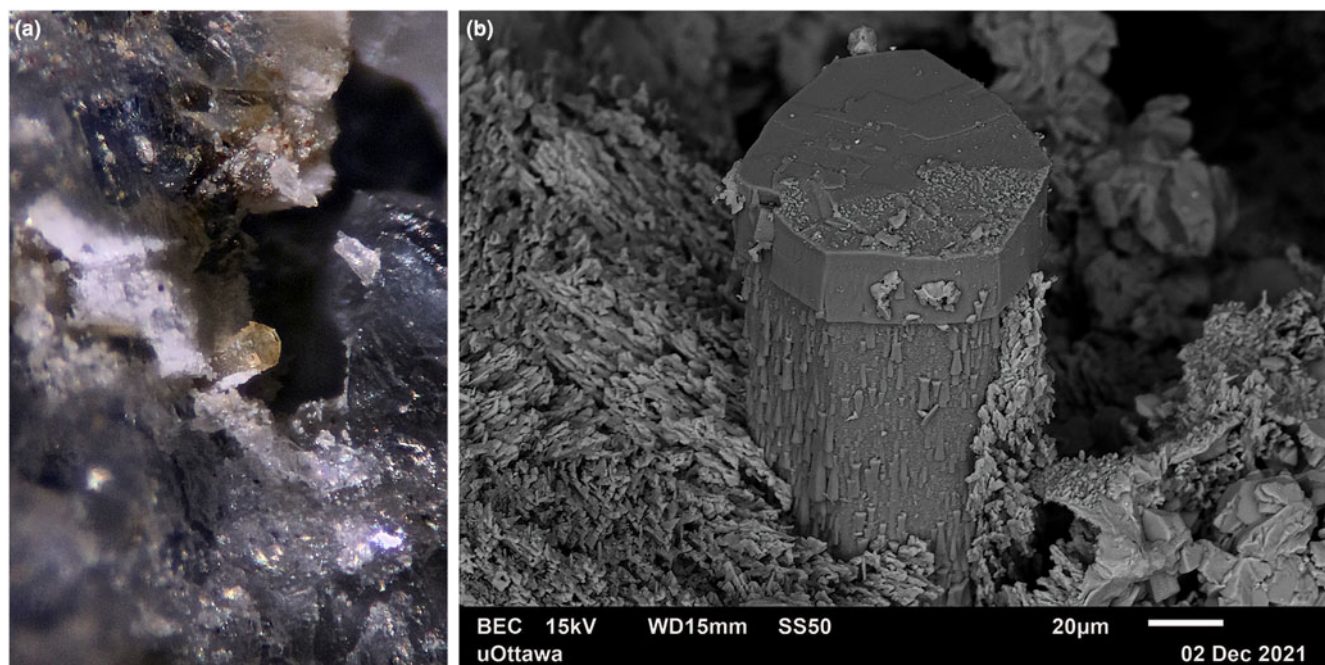
Fig. 19. (a) Photomicrograph of quintinite from Mount Mather Creek. Field of view = 2 mm, crystal = 80 × 60 μm (copyright Q. Wight; CMNMC 90163). (b) Back-scattered electron images of single crystals of quintinite showing the characteristic epitactic "cap". The quintinite is coated by a druse of calcite (CMNMC 90164).

into early apatite as well as crystallisation of Na-bearing silicate minerals (Giebel *et al.*, 2019). The presumed association of the Mount Mather Creek breccia to an unknown carbonatite or syenite parental body, together with its mineralogy suggests crystallisation from a SiO_2-undersaturated melt enriched in Na as well as Cl^-, OH^- and CO_3^{2-}, all of which contribute to high degrees of REE mobility in both the silicate and carbonate fraction and crystallisation of REE-bearing minerals in a brecciated dyke located distal to the parental intrusion. The presence of the Al-hydroxide nordstrandite in the late stages of crystallisation also supports crystallisation from a SiO_2-undersaturated melt.

Two sources are possible: (1) *in situ* exsolution of fluids from the crystallising silica-bearing carbonate melt or (2) infiltration of late-stage, fractionated carbonatitic fluids. If a highly evolved and fractionated silica-rich carbohydrothermal origin is invoked for the Mount Mather Creek breccia, cooling of this melt to temperatures at which ancylite-(Ce) is stable (<450°C), would result in formation of H_2O and CO_2-rich fractions. Large-ion incompatible elements such as Ba, Sr and LREE, excluded from earlier crystallising silicate phases (sodalite and microcline), would partition preferentially into the CO_2-rich fraction, resulting in co-precipitation of minerals such as ancylite-(Ce) and barytocalcite, whereas the alkali-rich H_2O fraction would result in the alteration of sodalite and precipitation of late-stage zeolites including albite, edingtonite, cancrinite, analcime, chabazite-Na and gonnardite. The lack of early-stage REE-bearing phosphates (britholite) or Na–Sr–REE carbonates (burbankite and carbocernaite) at Mount Mather Creek, minerals commonly observed in other carbonatite and carbohydrothermal deposits (Wall and Mariano, 1995; Zaitsev *et al.*, 1998; Wall and Zaitsev, 2004; Zaitsev *et al.*, 2014; Cooper *et al.*, 2015) precludes the possibility of remobilisation of REE from precursor minerals and favours a model which involves concentration of REEs in the late-stage fluid prior to ancylite-(Ce) formation. Similarly, the absence of REE

fluorocarbonates such as bastnäsite, parisite and synchysite commonly noted in other carbonatites (Ngwenya, 1994; Schultz *et al.*, 2004; Dalsin *et al.*, 2015; Andersen *et al.*, 2017; Giebel *et al.*, 2017), and the predominance of sodalite in the silicate fraction, indicate that the Mount Mather Creek system fluids had $Cl^- > F^-$. This is in contrast to carbohydrothermal deposits such as the Ashram (Mitchell and Smith, 2017), Rock Creek Canyon (Hoshino *et al.*, 2017) and Bayan Obo (Le Bas *et al.*, 1992) deposits which are dominated by fluids with $F^- > Cl^-$ with abundant fluorite and quartz in addition to REE carbonates. Late-stage baryte and Sr-bearing calcite after barytocalcite and calcite are post-magmatic minerals, the result of remobilisation of Ba and Sr from barytocalcite. Late-stage vug-filling minerals indicate the existence of post-magmatic fluids enriched in OH^-, Ca and Na as evidenced by the presence of the rare mineral quintinite, drusy calcite and chabazite-Na.

Conclusions

The Mount Mather Creek breccia is a carbohydrothermal deposit, the product of a medium temperature (<450°C), highly evolved, alkaline, SiO_2-undersaturated, Na–Ba–REE–Cl-rich, residual carbonated silicate melt whose parental origins are unknown. The deposit consists of a primary assemblage of concomitant calcite, ferroan dolomite, sodalite and microcline, with a secondary assemblage of LREE–Ba–Sr-bearing minerals including ancylite-(Ce), baryte, barytocalcite, Sr-rich calcite, edingtonite and a potentially new Mg-edingtonite mineral. It is also the second known Canadian locality for the layered double hydroxide, quintinite. Of note is the absence of many characteristic *bona fide* carbonatite minerals, including Nb–Ta oxides, REE-fluorocarbonates, magnetite, monazite, or ilmenite. Although no parental intrusion is evident on the surface, the mineralogy and texture of the breccia veins are similar to those

observed in other carbohydrothermal deposits associated with sodic peralkaline syenites including late stage 'carbonatite' veins observed in other parts of the British Columbia Alkaline Province.

References

Al Ani T. and Sarapää O. (2013) Geochemistry and mineral phases of REE in Jammi carbonatite veins and fenites, southern end of the Sokli complex, NE Finland. *Geochemistry: Exploration, Environment, Analysis*, **13**, 217–224.

Andersen A.K., Clark J.G., Larson P.B. and Donovan J.J. (2017) REE fractionation, mineral speciation, and supergene enrichment of the Bear Lodge carbonatites, Wyoming, USA. *Ore Geology Reviews*, **89**, 780–807.

Anenburg M., Mavrogenes J.A., Frigo C. and Wall F. (2020) Rare earth element mobility in and around carbonatites controlled by sodium, potassium, and silica. *Science Advances*, **6**, 10.

Armstrong J.T. (1988) Quantitative analysis of silicate and oxide minerals: Comparison of Monte Carlo, ZAP and phi-rho-Z procedures. Pp. 239–246 in *Microbeam Analysis* (D.E. Newbury, editor). San Francisco Press, USA.

Barnhisel R. and Rich C. (1965) Gibbsite, bayerite, and nordstrandite formation as affected by anions, pH, and mineral surfaces. *Soil Science Society of America Journal*, **29**, 531–534.

Chai L. and Navrotsky A. (1996) Synthesis, characterization, and energetics of solid solution along the dolomite-ankerite join, and implications for the stability of ordered CaFe(CO$_3$)$_2$. *American Mineralogist*, **81**, 1141–1147.

Chakhmouradian A.R., Reguir E.P., Couëslan C. and Yang P. (2016) Calcite and dolomite in intrusive carbonatites. II. Trace-element variations. *Mineralogy and Petrology*, **110**, 361–377.

Chang L.Y., Howie R.A. and Zussman J. (1996) *Rock Forming Minerals, Volume 5B: Non-silicates: sulphates, carbonates, phosphates and halides*. Longman, Harlow, UK, 383 pp.

Chao G.Y. and Baker J. (1982) Nordstrandite from Mont St-Hilaire, Quebec. *The Canadian Mineralogist*, **20**, 77–85.

Chao G.Y. and Gault R.A. (1997) Quintinite-2*H*, quintinite-3*T*, charmarite-2*H*, charmarite-3*T* and caresite-3*T*, a new group of carbonate minerals related to the hydrotalcite-manasseite group. *The Canadian Mineralogist*, **35**, 1541–1549.

Cooper A.F. (1996) Nb-rich baotite in carbonatites and fenites at Haast River, New Zealand. *Mineralogical Magazine*, **60**, 473–482.

Cooper A.F., Collins A.K., Palin J.M. and Spratt J. (2015) Mineralogical evolution and REE mobility during crystallisation of ancylite-bearing ferrocarbonatite, Haast River, New Zealand. *Lithos*, **216**, 324–337.

Costanzo A., Moore K.R., Wall F. and Feely M. (2006) Fluid inclusions in apatite from Jacupiranga calcite carbonatites: evidence for a fluid-stratified carbonatite magma chamber. *Lithos*, **91**, 208–228.

Currie K.L. (1976) The alkalkine rocks of Canada. *Geological Survey of Canada Bulletin*, **239**, 1–228.

Dalsin M., Groat L., Creighton S. and Evans R. (2015) The mineralogy and geochemistry of the Wicheeda carbonatite complex, British Columbia, Canada. *Ore Geology Reviews*, **64**, 523–542.

Drüppel K. (2003) *Petrogenesis of the Mesoproterozoic anorthosite, syenite and carbonatite suites of NW Namibia and their contribution to the metasomatic formation of the Swartbooisdrif sodalite deposits*. Universität Würzburg.

Drüppel K., Hoefs J. and Okrusch M. (2005) Fenitizing processes induced by ferrocarbonatite magmatism at Swartbooisdrif, NW Namibia. *Journal of Petrology*, **46**, 377–406.

Dunning G.E., Walstrom R.E. and Lechner W. (2018) Barium silicate mineralogy of the western margin, North American continent - part geology, origin,

paragenesis and mineral distribution from Baja California Norte, Mexico, Western Canada and Alaska, USS. *Baymin Journal*, **19**, 70.

Finch A.A. (1991) Conversion of nepheline to sodalite during subsolidus processes in alkaline rocks. *Mineralogical Magazine*, **55**, 459–463.

Gabrielse H. and Yorath C.J. (1991) Tectonic Synthesis. In: *Geology of the Cordilleran Orogen in Canada* (Gabrielse H. and Yorath C.J., editors). Geology of North America, Vol. G2, Geological Society of America.

Gatta G. and Boff Ballaran T. (2004) New insight into the crystal structure of orthorhombic edingtonite: evidence for a split Ba site. *Mineralogical Magazine*, **68**, 167–175.

Giebel R.J., Gauert C.D., Marks M.A., Costin G. and Markl G. (2017) Multi-stage formation of REE minerals in the Palabora Carbonatite Complex, South Africa. *American Mineralogist*, **102**, 1218–1233.

Giebel R., Parsapoor A., Walter B., Braunger S., Marks M., Wenzel T. and Markl G. (2019) Evidence for magma–wall rock interaction in carbonatites from the Kaiserstuhl Volcanic Complex (Southwest Germany). *Journal of Petrology*, **60**, 1163–1194.

Grand L.-M., Palmer S. and Frost R. (2010) Synthesis and thermal stability of hydrotalcites containing manganese. *Journal of Thermal Analysis and Calorimetry*, **100**, 981–985.

Green C., Simandl G.J., Paradis S., Katay F., Hoshino M., Kon Y., Kodama S. and Graf C. (2017) Geological setting of the Rock Canyon Creek REE-fluorite deposit, British Columbia, Canada. Pp. 195–203 in: *Geological Fieldwork 2016*, **2017-1**. British Columbia Ministry of Energy and Mines, British Columbia Geological Survey, Canada.

Grice J.D., Gault R.A. and Ansell H.G. (1984) Edingtonite: the first two Canadian occurrences. *The Canadian Mineralogist*, **22**, 253–258.

Hatert F. and Burke E.A. (2008) The IMA–CNMNC dominant-constituent rule revisited and extended. *The Canadian Mineralogist*, **46**, 717–728.

Hey M.H. (1950) *An index of mineral species & varieties arranged chemically: with an alphabetical index of accepted mineral names and synonyms*. British Museum, London.

Hogarth D.D. (1989) Pyrochlore, apatite and amphibole: distinctive minerals in carbonatite. Pp. 105–148 in: *Carbonatites: Genesis and Evolution* (K. Bell, editor). Unwin Hyman, London.

Hora Z.D. and Hancock K.D. (1996) A new sodalite occurrence: Mount Mather Creek, British Columbia (82N/lOW). Pp. 317–320 in: *British Columbia Geological Survey Fieldwork 1996*, **1997-1**. British Columbia Ministry of Energy and Mines, British Columbia Geological Survey, Canada.

Horváth L. (2010) The minerals of the Saint-Amable sill: an update. *Micronews*, **44**, 23–28.

Horváth L., Gault R., Pfenniger-Horváth E. and Poirier G. (2019) *Mont Saint-Hilaire: History, Geology and Mineralogy*. Mineralogical Association of Canada, Quebec, Canada, 644 pp.

Hoshino M., Kon Y., Kodama S., Simandl G.J., Paradis S., Green C., Namatame C., Matsunaga I. and Takagi T. (2017) Mineralogy of the Rock Canyon Creek REE-fluorite deposit, British Columbia, Canada. Pp. 205–213 in: *Geological Fieldwork 2016, 2017-1*. British Columbia Ministry of Energy and Mines, British Columbia Geological Survey, Canada.

Kapustin Y.L. (1980) *Mineralogy of Carbonatites*. Amerind Publishing, New Dehli, India, 259 pp.

Kawano M. and Tomita K. (1996) Amorphous aluminum hydroxide formed at the earliest weathering stages of K-feldspar. *Clays and Clay Minerals*, **44**, 672–676.

Knudsen C. (1991) *Petrology, Geochemistry and Economic Geology of the Qaqarssuk Carbonatite Complex, Southern West Greenland*. Mineral Deposits, Vol. 29. Gebrüder Borntraeger, Stuttgart, Germany, 110 pp.

Kovács-Pálffy P., Velledits F., Kónya P., Földvári M. and Gálné Sólymos K. (2008) Nordstrandite - a new occurrence from Hungary. *Acta Mineralogica-Petrographica*, **48**, 43–48.

Larsen A.O. (2010) *The Langesundsfjord – History, Geology, Pegmatites, Minerals*. Bode Verlag, Salzhemmendorf, Germany, 239 pp.

Lasley S. (2021) *Canada set to be Critical Minerals Store*. North of 60 Mining News, Eagle River, Alaska, USA.

Le Bas M., Kellere J., Kejie T., Wall F., William C. and Peishan Z. (1992) Carbonatite dykes at bayan Obo, inner Mongolia, China. *Mineralogy and Petrology*, **46**, 195–228.

Le Maitre R. (2002) *Igneous Rocks: A Classification and Glossary of Terms: Recommendations of the IUGS, Subcommission on the Systematics of Igneous rocks*. 2nd Edition. Cambridge University Press, Cambridge, UK, 236 pp.

McDonough W.F. and Sun S.s. (1995) The composition of the Earth. *Chemical Geology*, **120**, 223–253.

Mills S.J., Christy A.G., Génin J.-M., Kameda T. and Colombo F. (2012) Nomenclature of the hydrotalcite supergroup: natural layered double hydroxides. *Mineralogical Magazine*, **76**, 1289–1336.

Mitchell R.H. (2005) Carbonatites and carbonatites and carbonatites. *The Canadian Mineralogist*, **43**, 2049–2068.

Mitchell R.H. and Smith D.L. (2017) Geology and mineralogy of the Ashram Zone carbonatite, Eldor Complex, Québec. *Ore Geology Reviews*, **86**, 784–806.

Nadeau O., Cayer A., Pelletier M., Stevenson R. and Jébrak M. (2015) The Paleoproterozoic Montviel carbonatite-hosted REE–Nb deposit, Abitibi, Canada: Geology, mineralogy, geochemistry and genesis. *Ore Geology Reviews*, **67**, 314–335.

Natural Resources Canada (2021) *Rare Elements Facts*. Natural Resources Canada, Government of Canada, Ottawa, https://www.nrcan.gc.ca/our-natural-resources/minerals-mining/minerals-metals-facts/rare-earth-elements-facts/20522.

Ngwenya B.T. (1994) Hydrothermal rare earth mineralisation in carbonatites of the Tundulu complex, Malawi: processes at the fluid/rock interface. *Geochimica et Cosmochimica Acta*, **58**, 2061–2072.

Nickel E.H. and Grice J.D. (1998) The IMA Commission on New Minerals and Mineral Names: procedures and guidelines on mineral nomenclature, 1998. *Mineralogy and Petrology*, **64**, 237–263.

Pekov I.V. (2000) *Lovozero Massif: History, Pegmatites, Minerals*. Pp. 479. Vneshtorgizdat, Moscow, Russia.

Pell J. (1994) Carbonatite, nepheline syenites, kimberlites and related rocks in British Columbia. *Mineral Resource Division Bulletin*, **88**. Province of British Columbia Ministry of Energy, Mines and Petroleum Resources, Canada.

Peskleway C.D., Henderson G.S. and Wicks F.J. (2005) Growth of nordstrandite: effect of chloride on surface morphology. *Journal of Crystal Growth*, **273**, 614–623.

Petersen O., Johnsen O. and Leonardsen E. (1976) Nordstrandite from Narssârssuk, Greenland. *The Mineralogical Record*, **7**, 78–82.

Petersen O., Niedermayr G., Gault R., Brandstatter F., Micheelsen H. and Giester G. (2001) Ancylite-(La) from the Ilimaussaq alkaline complex, South Greenland. *Neues Jahrbuch für Mineralogie Monatshefte*, 493–504.

Peterson T. and Currie K. (1994) The Ice River Complex, British Columbia. *Geological Survey of Canada Current Research A*, **1994**, 185–192.

Platt R.G. and Woolley A.R. (1990) The carbonatites and fenites of Chipman Lake, Ontario. *The Canadian Mineralogist*, **28**, 241–250.

Raade G. (2013) Hydrotalcite and quintinite from Dypingdal, Snarum, Buskerud, Norway. *Norsk Bergverksmuseum Skrifter*, **50**, 55–57.

Ramesh T.N. (2012) Polytypic transformations of aluminum hydroxide: A mechanistic investigation. *Particuology*, **10**, 359–364.

Reeder R.J. and Dollase W.A. (1989) Structural variation in the dolomite-ankerite solid-solution series; an X-ray, Moessbauer, and TEM study. *American Mineralogist*, **74**, 1159–1167.

Reguir, E. and Mitchell, R. (2000) The mineralogy of carbonatites and related potassic syenites from the Rocky Boy stock, Bearpaw Mountains, north-central Montana. *Proceedings of the GeoCanada 2000 Conference*, Calgary, Canada.

Rosenberg P. (1967) Subsolidus relations in the system $CaCO_3$-$MgCO_3$-$FeCO_3$ between 350 and 550 °C. *American Mineralogist*, **52**, 787–796.

Rosenberg P. (1968) Subsolidus relations on the dolomite join, CaMg $(CO_3)_2$-$CaFe(CO_3)_2$-$CaMn(CO_3)_2$. *American Mineralogist*, **53**, 880–889.

Rowe R. (2009) New statistical callibration approach for Bruker AXS D8 Discover microdiffractometer with Hi-Star detector using GADDS software. *Powder Diffraction*, **24**, 263–271.

Sabina A. (1982) Some rare minerals of the Bancroft area. *The Mineralogical Record*, **13**, 223–228.

Schultz F., Lehmann B., Tawackoli S., Rössling R., Belyatsky B. and Dulski P. (2004) Carbonatite diversity in the Central Andes: the Ayopaya alkaline province, Bolivia. *Contributions to Mineralogy and Petrology*, **148**, 391–408.

Sharp Z., Helffrich G., Bohlen S.R. and Essene E.J. (1989) The stability of sodalite in the system $NaAlSiO_4$–NaCl. *Geochimica et Cosmochimica Acta*, **53**, 1943–1954.

Simandl G.J. and Clarke G. (2016) Rare Metals. *British Columbia Geological Survey Information Circular*, 2016-4, BC Geological Survey, Mineral Development Office, Vancouver, Canada.

Simandl G., Prussin E., Hankock K. and Meredith Jones S. (2012) Rare metal-bearing deposits in British Columbia with selected examples. *British Columbia Geological Survey Geofile*, 2012–02. British Columbia Ministry of Energy and Mines, Vancouver, Canada.

Simandl G.J., Paradis S., Savard J., Miller D., D'Souza R., Araoka D., Akam C., Hoshino M. and Kon Y. (2021) Mineral control on the geochemistry of the Rock Canyon Creek REE-F-Ba deposit, British Columbia, Canada. *Geochemistry: Exploration, Environment, Analysis*, **21**, 1–20.

Sørensen H. (1958) The Ilímaussaq batholith - a review and discussion. *Meddr Grønland*, **181**, 1–32.

Stormer J.C., Pierson M.L. and Tacker R.C. (1993) Variation of F and Cl X-ray intensity due to anisotropic diffusion in apatite during electron microprobe analysis. *American Mineralogist*, **78**, 641–648.

Strand U. (2016) Quintinit-2*H*, ett nytt mineral för Långban. *LångbansNytt*, **22**, 21–23.

Traversa G., Gomes C.B., Brotzu P., Buraglini N., Morbidelli L., Principato M.S., Ronca S. and Ruberti E. (2001) Petrography and mineral chemistry of carbonatites and mica-rich rocks from the Araxá complex (Alto Paranaíba Province, Brazil). *Anais da Academia Brasileira de Ciências*, **73**, 71–98.

Vartiainen H. (1980) The petrography, mineralogy and petrochemistry of the Sokli carbonatite massif, northern Finland. *Bulletin of Geological Survey of Finland*, **313**. Espoo, Finland.

Violante A. and Huang P. (1993) Formation mechanism of aluminum hydroxide polymorphs. *Clays and Clay Minerals*, **41**, 590–597.

Vlasov K. A., Kuz'menko M. and Es′kova E.M. (1966) *The Lovozero Alkali Massif*. (Transl. from U.S.S.R. Acad. Sci. Press, Moscow, 1959) Hafner Publishing Company, New York.

Wall F. and Mariano A. (1995) Rare earth minerals in carbonatites: a discussion centred on the Kangankunde Carbonatite, Malawi. *Mineralogical Society Series*, **7**, 193–226.

Wall F. and Zaitsev A.N. (2004) Rare earth minerals in Kola carbonatites. Pp. 43–72 in: *Phoscorites and Carbonatites From Mantle To Mine: The Key Example of The Kola Alkaline Province*. The Mineralogical Society Series, Volume 10. The Mineralogical Society of Great Britain and Ireland, London.

Warr L.N. (2021) IMA–CNMNC approved mineral symbols. *Mineralogical Magazine*, **85**, 291–320. doi:http://dx.doi.org/10.1180/mgm.2021.43.

Woolley A.R. (2019) *Alkaline Rocks and Carbonatites of the World Part 4: Antarctica Asia and Europe (excluding the former USSR), Australasia and Oceanic Islands*. Geological Society of London, London.

Yakovenchuk V.N., Ivanyuk G., Pakhomovsky Y. and Men'shikov Y. (2005) *Khibiny*. Laplandia Minerals in association with the Mineralogical Society of Great Britain and Ireland, Apatity & London, 468 pp.

Zaitsev A.N. (1996) Rhombohedral carbonates from carbonatites of the Khibina massif, Kola Peninsula, Russia. *The Canadian Mineralogist*, **34**, 453–468.

Zaitsev A.N., Wall F. and Le Bas M.J. (1998) REE-Sr-Ba minerals from the Khibina carbonatites, Kola Peninsula, Russia: their mineralogy, paragenesis and evolution. *Mineralogical Magazine*, **62**, 225–250.

Zaitsev A.N., Williams T.C., Jeffries T.E., Strekopytov S., Moutte J., Ivashchenkova O.V., Spratt J., Petrov S.V., Wall F., Seltmann R. and Borozdin A.P. (2014) Rare earth elements in phoscorites and carbonatites of the Devonian Kola Alkaline Province, Russia: Examples from Kovdor, Khibina, Vuoriyarvi and Turiy Mys complexes. *Ore Geology Reviews*, **61**, 204–225.

Zhitova E.S., Popov M.P., Krivovichev S.V., Zaitsev A.N. and Vlasenko N.S. (2017) Quintinite-1*M* from the Mariinsky Deposit, Ural Emerald Mines, Central Urals, Russia. *Geology of Ore Deposits*, **59**, 745–751.

Zhitova E.S., Krivovichev S.V., Yakovenchuk V.N., Ivanyuk G.Y., Pakhomovsky Y.A. and Mikhailova J.A. (2018) Crystal chemistry of natural layered double hydroxides: 4. Crystal structures and evolution of structural complexity of quintinite polytypes from the Kovdor alkaline-ultrabasic massif, Kola peninsula, Russia. *Mineralogical Magazine*, **82**, 329–346.